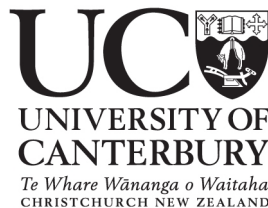


Simulation of Cascades for the IceCube Neutrino Telescope

A THESIS SUBMITTED IN PARTIAL FULFILMENT
OF THE REQUIREMENTS FOR THE DEGREE OF
MASTER OF SCIENCE

Stephanie Hickford

2007



Abstract

Neutrino telescopes open a new observational window on the universe. Neutrino interactions in these detectors can give rise to a combination of electromagnetic cascades, hadronic cascades and long range muons. Cerenkov radiation from these products is detected by the neutrino telescope. In this thesis the observational signatures associated with various neutrino-nucleon interaction products are investigated. Cerenkov radiation is emitted at a distinctive angle, about 40° in ice. The maximum number of optical photons that can be produced per unit charged tracklength is calculated to be $562 \text{ photons cm}^{-1}$.

The simulation programs Pythia and GEANT are used to study neutrino interactions using ice as the medium. The production of tau from the tau neutrino interaction is considered and it is found that the Cerenkov angle from tau is not distinctive at low energies, due to its lifetime tau decays before travelling an observable distance. The energy required for a tau neutrino to produce a sharp tau Cerenkov signal is on the order of 1 PeV.

In a high energy electron neutrino interaction the resulting hadronic cascade contains high energy pions and kaons. These particles decay, often producing muons that are also high energy and therefore long range. Due to the muons travelling faster than the local speed of light in ice, their signal may be received by the detector earlier than the signal resulting from the event that created the muon. This can complicate the reconstruction of electron neutrino events.

Contents

Figures	iv
Tables	vii
1 Introduction	1
2 Neutrino Astronomy	4
2.1 Neutrinos as a window to the universe	4
2.2 Science motivation for neutrino telescopes	5
2.3 Description of neutrino telescopes	7
2.3.1 DUMAND	8
2.3.2 Baikal	8
2.3.3 NESTOR	9
2.3.4 ANTARES	9
2.3.5 AMANDA	9
2.3.6 IceCube	10
3 Physics of Neutrino Detection	11
3.1 Leptonic interactions	11
3.1.1 The electron neutrino interaction	12
3.1.2 The muon neutrino interaction	13
3.1.3 The tau neutrino interaction	14
3.2 Hadronic cascades	14
3.3 Cerenkov radiation	15
3.4 Optical photons	15

4	Simulation Programs	17
4.1	Pythia – The event generation	17
4.1.1	Initial and final state radiation	17
4.1.2	Multiple interaction among beam jets	18
4.1.3	Fragmentation	18
4.1.4	HEP subroutine	18
4.2	GEANT 4.8 – The event simulation	18
4.2.1	Hadronic and Cerenkov processes	18
4.2.2	Detector Construction	19
5	Detection of the Tau Lepton	20
5.1	Tau and the tau neutrino	20
5.2	Processes	21
5.2.1	Decay	21
5.2.2	Multiple scattering	21
5.2.3	Ionization	21
5.2.4	Bremsstrahlung and pair production	24
5.3	Cerenkov radiation from muons and taus	24
5.4	Range expectation for tau	27
6	Long Range Muon Production	29
6.1	High energy hadrons	29
6.2	Pion and kaon production from electron neutrino interactions	30
6.3	The y distribution	37
6.4	Pion and kaon decay	38
6.5	Muon Production from Decay of Pions and Kaons	40
7	Light Signal from Long Range Muons	45
7.1	Photons from long range muons	45
7.2	Light signal simulation	46

8 Summary and Conclusions	49
A Additional physics source code	52
B IceCube detector construction source code	55
C DOM timing source code	59
References	62
Acknowledgements	64

List of Figures

3.1	Electron, muon and tau neutrino interaction with a proton in a detector.	12
3.2	Bremsstrahlung and pair production in an electromagnetic cascade.	12
3.3	Bremsstrahlung in a hadronic cascade.	13
3.4	Example of tau decay.	14
5.1	Cerenkov angle for 10 GeV μ^-	25
5.2	Cerenkov angle for 10 GeV τ^-	25
5.3	Cerenkov angle for 20 GeV μ^-	25
5.4	Cerenkov angle for 20 GeV τ^-	25
5.5	Cerenkov angle for 30 GeV μ^-	25
5.6	Cerenkov angle for 30 GeV τ^-	25
5.7	Cerenkov angle for 40 GeV μ^-	26
5.8	Cerenkov angle for 40 GeV τ^-	26
5.9	Cerenkov angle for 50 GeV μ^-	26
5.10	Cerenkov angle for 50 GeV τ^-	26
6.1	Pions produced from one 10 TeV electron neutrino event.	31
6.2	Kaons produced from one 10 TeV electron neutrino event.	31
6.3	Pions produced from one 100 TeV electron neutrino event.	31
6.4	Kaons produced from one 100 TeV electron neutrino event.	31
6.5	Pions produced from one 500 TeV electron neutrino event.	31
6.6	Kaons produced from one 500 TeV electron neutrino event.	31
6.7	Pions produced from one 1 PeV electron neutrino event.	32
6.8	Kaons produced from one 1 PeV electron neutrino event.	32

6.9	Pions produced from one 2 PeV electron neutrino event.	32
6.10	Kaons produced from one 2 PeV electron neutrino event.	32
6.11	Pions produced from one hundred 10 TeV electron neutrino events.	32
6.12	Kaons produced from one hundred 10 TeV electron neutrino events.	32
6.13	Pions produced from one hundred 100 TeV electron neutrino events.	33
6.14	Kaons produced from one hundred 100 TeV electron neutrino events.	33
6.15	Pions produced from one hundred 500 TeV electron neutrino events.	33
6.16	Kaons produced from one hundred 500 TeV electron neutrino events.	33
6.17	Pions produced from one hundred 1 PeV electron neutrino events.	33
6.18	Kaons produced from one hundred 1 PeV electron neutrino events.	33
6.19	Pions produced from one hundred 2 PeV electron neutrino events.	34
6.20	Kaons produced from one hundred 2 PeV electron neutrino events.	34
6.21	Pions produced from ten thousand 10 TeV electron neutrino events.	34
6.22	Kaons produced from ten thousand 10 TeV electron neutrino events.	34
6.23	Pions produced from ten thousand 100 TeV electron neutrino events.	34
6.24	Kaons produced from ten thousand 100 TeV electron neutrino events.	34
6.25	Pions produced from ten thousand 500 TeV electron neutrino events.	35
6.26	Kaons produced from ten thousand 500 TeV electron neutrino events.	35
6.27	Pions produced from ten thousand 1 PeV electron neutrino events.	35
6.28	Kaons produced from ten thousand 1 PeV electron neutrino events.	35
6.29	Pions produced from ten thousand 2 PeV electron neutrino events.	35
6.30	Kaons produced from ten thousand 2 PeV electron neutrino events.	35
6.31	Comparison of our simulated y distribution to the theoretical y distribution calculated by Gandhi <i>et al.</i> [10].	37
6.32	Muons from pion decay for one 10 TeV electron neutrino event.	41
6.33	Muons from kaon decay for one 10 TeV electron neutrino event.	41
6.34	Muons from pions decay for one 100 TeV electron neutrino event.	41
6.35	Muons from kaon decay for one 100 TeV electron neutrino event.	41
6.36	Muons from pion decay for one 500 TeV electron neutrino event.	42
6.37	Muons from kaons decay for one 500 TeV electron neutrino event.	42

6.38	Muons from pion decay for one 1 PeV electron neutrino event.	42
6.39	Muons from kaon decay for one 1 PeV electron neutrino event.	42
6.40	Muons from pion decay for one hundred 10 TeV electron neutrino events. .	43
6.41	Muons from kaon decay for one hundred 10 TeV electron neutrino events. .	43
6.42	Muons from pion decay for one hundred 100 TeV electron neutrino events.	43
6.43	Muons from kaon decay for one hundred 100 TeV electron neutrino events.	43
7.1	Muon travelling 10° downwards from (-125,500).	47
7.2	Muon travelling 10° upwards from (-125,500).	47
7.3	Muon travelling 20° downwards from (-125,500).	47
7.4	Muon travelling 20° upwards from (-125,500).	47
7.5	Muon travelling 30° downwards from (-125,500).	47
7.6	Muon travelling 30° upwards from (-125,500).	47
7.7	Muon travelling 40° downwards from (-125,500).	48
7.8	Muon travelling 40° upwards from (-125,500).	48
7.9	Muon travelling 50° downwards from (-125,500).	48
7.10	Muon travelling 50° upwards from (-125,500).	48

List of Tables

3.1	Optical photons produced per centimetre of track length from Cerenkov radiation.	16
5.1	Basis decay modes and branching ratios for tau minus [12].	22
5.2	Comparison of simulated and calculated number of photons per centimetre of track length for a muon.	27
6.1	Number of pions and kaons and their mean energy in our Pythia simulations.	36
6.2	Our simulated values and theoretical values calculated by Gandhi <i>et al.</i> [10] for the y distribution.	38
6.3	Decay modes with high branching ratios for pions [12].	39
6.4	Decay modes with high branching ratios for kaons [12].	39
6.5	Number of muons and their mean energies produced from pion and kaon decay.	44
6.6	Highest energy muons from pion and kaon decay.	44

Chapter 1

Introduction

Neutrinos, discovered in 1956 [21], have led to progress in our understanding in many areas of science. First postulated in 1930, neutrinos remained undetected experimentally for over 20 years due to their elusive nature. A neutrino is a chargeless and stable lepton and interacts only by the weak interaction. Three flavours of neutrinos have been detected, all with very small masses, corresponding to the three flavours of charged leptons.

Neutrinos open an observational window to our universe which has begun to be explored over the last 30 years. Neutrinos reach us on earth directly from their source, losing no information through interactions on their way. It is for this reason that using neutrinos to observe the universe may lead to new discoveries and neutrino astrophysics will heighten understanding of many phenomena throughout the universe. Though neutrinos provide a useful method to observe the universe, they are difficult to detect because of their extremely weak interaction with matter. This thesis is concerned with examining the observational signals for neutrinos in a neutrino telescope with ice as its detecting medium.

Neutrino telescopes are situated hundreds of metres under water or ice where the signal to noise ratio for neutrino interactions is improved. The major noise sources are muons that are produced when cosmic rays interact in the earth's atmosphere and neutrinos produced in the atmosphere. While these are themselves interesting to study, it is the neutrinos originating from far outside our galaxy that we are most interested in, and that the larger telescopes aim to detect. The detection of these high energy neutrinos will allow us a better understanding of many phenomena. The origin of high energy cosmic rays is an important question that is being addressed, as the mechanism that accelerates these cosmic rays is not yet understood. Neutrinos are expected to be produced in dense regions with high gravitational fields [15]. They travel straight to earth and then interact in large

neutrino telescopes. Some poorly understood phenomena in these sorts of regions of the universe include gamma ray bursts, supernova bursts, active galactic nuclei and supernova remnants. The high energy neutrinos that we detect will provide more information in these areas and may reveal new phenomena that have not yet been observed. These detectors will help us to learn more about properties of neutrinos such as neutrino oscillation, and possibly exotic particles such as WIMP candidates and magnetic monopoles.

When arriving at the detectors, high energy neutrinos interact with protons in the surrounding medium via exchange of Z or W^\pm bosons producing their charged leptonic partner. This charged lepton travels through the detector away from the interaction point. Each charged lepton creates a distinct detector signal [15]. Only muons travel a significant distance in the ice travelling past optical modules faster than the local speed of light, thereby emitting Cerenkov radiation. This is a cone of light expanding through the detector triggering the optical modules as it passes. Taus and electrons do not travel very far before initiating a cascade of particles. The proton will shatter into its constituents and continue to fragment causing a hadronic cascade containing many different hadronic and leptonic particles. These particles can also emit Cerenkov radiation observed by optical modules. This hadronic cascade can be reconstructed giving further information about the original neutrino. These optical modules turn light signals into electrical pulses and sends the information to the surface hundreds of metres above.

Although the work described here mainly concerns IceCube, the calculations and simulations are applicable to many neutrino telescopes, hence chapter two summarises many of the neutrino detectors constructed and operated by different institutes and collaborations around the world.

Chapter two, entitled Neutrino Astronomy, introduces neutrinos as an observational tool which may help solve some of the mysteries of the universe. The many diverse neutrino detectors built around the world are outlined in this chapter. Chapter three concerns the physics of neutrino detectors, and details the leptonic interactions and outlines optical Cerenkov radiation which is the process neutrino detectors use to observe neutrino interactions. Chapter four outlines the simulation programs used in the subsequent work. Chapter five is a study of the detection of the tau neutrino. This is an interaction which is not observed as frequently as the others due to the nature of the tau lepton. This chapter contains results from simulations looking at this interaction in detail, particularly in comparison to the muon neutrino interaction. Chapter six is a detailed study of pion and kaon production in an electron neutrino interaction. This chapter looks at the decay of pions and kaons into muons. The detection of these muons that can be misinterpreted

in the reconstruction of electron neutrino cascade events. Chapter seven is a study of the light signal received by the optical modules in the IceCube neutrino telescope from long range muons. These signals are used in the reconstruction and analysis of events. Chapter eight summarises the key results and concludes this thesis.

Chapter 2

Neutrino Astronomy

In this chapter we describe how detecting neutrinos opens a new observational window to the universe. Neutrino processes and the phenomena that may be observed using neutrinos are described. This is followed with an outline of various neutrino telescopes situated around the globe.

2.1 Neutrinos as a window to the universe

For centuries scientists have progressively looked out at the universe using different wavelength bands of electromagnetic radiation. Originally the universe was observed using visible light, then observations progressed to other wavelengths such as radio waves, microwaves, infrared, ultra violet, x-rays and gamma-rays. Each part of the electromagnetic spectrum we use to observe our surroundings allows us to observe more of the universe and understand better what has been observed before. More diverse methods of observing the universe have allowed us to discover new phenomena and to give insight into new theories of the origins of the universe.

Neutrino detection offers another observational window into our diverse universe. Neutrinos are leptons, but unlike their counterparts, the electron, the muon and the tau, neutrinos have no electric charge. This means that they are not affected by electric and magnetic fields that permeate throughout space. A neutrino will travel in a straight line from its source to reach us on earth and hence contain directional information about its origin. Neutrinos are also only weakly interacting. In travelling to our detectors a neutrino will undergo few interactions and reach our detectors largely unaltered from when it was emitted from its source. Unfortunately, all these advantages of using neutrinos to observe the universe makes them very difficult to detect.

Despite the experimental challenge, neutrinos were first detected from an extragalactic source over 20 years ago. These neutrinos originated from supernova SN1987A, detected on the 24th February 1987. This supernova is 179,000 light years away from us, situated in the Tarantula nebula, a member of the Large Magellanic Cloud. The star that exploded was Sanduleak, a blue supergiant. According to theories of supernova energies, approximately 10 neutrinos should have been detected by each detector within 10 seconds. A total of 24 neutrinos were detected, 11 by Kamiokande II in Japan [14], 8 by IMB in the United States [4] and 5 by Baksan in Russia. This observation of neutrinos at three different sites around the globe gave the first indication that astronomy with neutrinos is a viable and informative way of observing extra galactic phenomena.

2.2 Science motivation for neutrino telescopes

Neutrino astronomy has the potential to advance science in many fields including astronomy, astrophysics, cosmology and particle physics. The neutrinos that we can observe are divided into two groups: low energy neutrinos and high energy neutrinos [9]. The lower energy end of the spectrum contains neutrinos that are produced in nuclear processes such as fusion reactions in the sun or in the centre of supernovae. The higher end of the neutrino spectrum contains neutrinos mostly produced in particle collisions where short lived mesons are produced which decay to neutrinos and other particles, or from the annihilation of heavy particles such as those hypothesised to constitute dark matter.

The production of high energy neutrinos occurs in regions in the universe containing astrophysical objects that emit large amounts of energy in various electromagnetic wavelengths. Short lived mesons are predicted to be produced in hadronic models for the production of electromagnetic radiation. These dense regions of the universe with large gravitational forces which generate relativistic jets where particles would be accelerated. Neutrinos will be produced from pions produced in hadronic collisions. This process is shown below,

$$\begin{aligned}
 p + p/\gamma &\rightarrow \pi^0 + \text{anything} \\
 &\searrow 2\gamma
 \end{aligned}
 \tag{2.1}$$

$$\begin{aligned}
 p + p/\gamma &\rightarrow \pi^\pm + \text{anything} \\
 &\searrow \mu^+ + \nu_\mu \quad (\mu^- + \bar{\nu}_\mu) \\
 &\quad \searrow e^+ + \nu_e + \bar{\nu}_\mu \quad (e^- + \bar{\nu}_e + \nu_\mu).
 \end{aligned}
 \tag{2.2}$$

It is this regime of high energy neutrinos that is of interest and detectable by telescopes like IceCube with one goal being learning about the high energy objects that produced them.

Neutrino telescopes may allow us to learn more about some of the sources of high energy radiation which include:

- High energy neutrinos originating from transient sources. These sources may include Gamma Ray Bursts (GRBs) and supernova bursts. GRBs last from a few milliseconds to several minutes and are the most energetic form of light we observe in the universe. The majority of energy from supernova bursts is released in a small time frame of about ten seconds.
- High energy neutrinos originating from steady and variable sources. These may include Active Galactic Nuclei (AGN) or supernova remnants (SNR). AGNs are the extremely bright cores of galaxies which may be attributed to super massive black holes. There is an excess of energy emitted from AGNs in many of the electromagnetic wavelength bands that we detect. This implies there may also be observable neutrinos emitted from these objects. SNRs are the source and distributor of heavy elements throughout the universe. Looking at the neutrinos produced in these regions may give us an insight to the mechanisms at work in SNRs.
- Sources of cosmic rays. We observe high energy cosmic rays up to 3×10^{20} eV. There is no known mechanism that can accelerate cosmic rays to this energy. Looking in the direction that neutrinos in cosmic rays originate may give insight to the origin of phenomena capable of this type of acceleration.

Examples of neutrinos produced by annihilation and exotic physics which IceCube can seek to detect include:

- Weakly Interacting Massive Particles (WIMPs). These have the characteristics to be dark matter candidates. WIMPs may be captured by the gravitational attraction of the sun or the earth and cluster at their centres. Here they would undergo annihilation and produce neutrinos that we may detect. These observations may put limits on the properties of WIMPs or rule out some models altogether.
- Neutrino oscillation. The production of tau neutrinos in hadronic interactions is suppressed compared to that of electron neutrinos and muon neutrinos. This means there will be fewer tau neutrinos produced from galactic or extra galactic sources.

The ratio of tau neutrinos compared to that of the other neutrino flavours can give information about the mixing of neutrino flavours.

- Neutrinos produced from the decay of super heavy particles. This is related to topological defects originating from phase transitions in the early universe.
- The search for magnetic monopoles and other exotic particles. This may include strange quark matter. Magnetic monopoles travelling close to the speed of light in vacuum would emit Cerenkov light which is detectable in the same manner as other charged particles. This Cerenkov light would exceed that of the light emitted from a muon and so the signal would be unique and distinguishable from other interactions.

Furthermore, IceCube will monitor the galaxy for MeV neutrinos from supernova explosions. This operates in the worldwide Supernova Early Warning System (SNEWS) triangulation network. This system uses the neutrino detectors around the world that are sensitive to supernova neutrino signal in our galaxy. This network provides an early warning of supernova occurrences so that astronomers may search for an optical counterpart.

IceCube may also reveal unexpected phenomena. With each new technique of observing the universe there are unanticipated surprises and observations which lead to exciting new science. It is hoped that neutrino astronomy will be no exception.

2.3 Description of neutrino telescopes

Many neutrino telescopes have been constructed around the globe. All these neutrino detectors need a large effective area to overcome the small neutrino cross section with matter and the lower flux at energies of interest. Those that have underground tanks of water include IMB, Super-Kamiokande, Borexino, KamLand, Frejus, MACRO and Soudan. These neutrino detectors look at neutrino properties using neutrinos that originate from the sun, the atmosphere or nuclear reactors.

The neutrino spectrum is expected to extend in energy beyond 10^{20} eV and originate from all directions in the sky [9]. Neutrino telescopes have to be constructed in environmental conditions where neutrino interactions with the surrounding medium are detectable, and background noise is minimised. There are billions of neutrinos passing through a detector at any time, some from galactic or extra galactic sources and many from local sources such as neutrinos produced in atmospheric interactions. The detection of neutrinos originating from a cosmic source rather than a local source should be made as

favourable as possible. In order to achieve this many neutrino telescopes have been built deep under water or ice. These neutrino telescopes include DUMAND, Baikal, NESTOR, ANTARES, AMANDA and IceCube. Neutrino telescopes that are located far below the surface may look at only neutrinos travelling upward through the earth. This is advantageous because the atmospheric muon background produced in the opposite hemisphere is not likely to travel all the way through the earth to the detector. The latter two neutrino telescopes, AMANDA and IceCube use ice as the medium rather than water.

Neutrino telescopes use arrays of photomultiplier tubes to detect the light from particles travelling through them. The photomultiplier tubes are attached to strings that are lowered under the surface of the water or ice. These photomultiplier tubes capture and convert real time light signals in the medium, into electrical pulses. This information is stored and transmitted to the surface. The arrival time of individual photons can be obtained to within a few nanoseconds and this data is used for event reconstruction and analysis.

2.3.1 DUMAND

DUMAND is the Deep Underwater Muon And Neutrino Detection telescope [17] operated from the University of Hawaii on the Island of Oahu. DUMAND was one of the first deep ocean high energy neutrino detector project and existed from 1976 to 1995. DUMAND was located at a depth of 4760 m in the Pacific Ocean at Keahole Point, 30 km off the coast of the Big Island of Hawaii. The DUMAND telescope was used to carry out many studies, including analysis of the first neutrino detector technology and ocean optics. DUMAND used a prototype of vertical strings of instruments deployed from a special ship. This experiment demonstrated the technology for deep underwater neutrino detection was possible, and succeeded in measuring the cosmic ray muon flux in the deep ocean. One of DUMANDs successes was to set the then best limits on PeV neutrinos that are expected from Active Galactic Nuclei. This first experiment laid the path for many other deep underwater and ice neutrino detectors.

2.3.2 Baikal

The Baikal collaboration consists of Russian and German institutes including INR Moscow, Irkutsk State University, Moscow State University and DESY, Zeuthen. The Baikal telescope was constructed in 1993 and upgraded to the NT-200 telescope consisting of 192 optical modules in 1998 [25]. The Baikal experiment uses a three dimensional grid with

several strings attached at the centre forming an umbrella like shape, and is located in the southern part of the freshwater Lake Baikal at a depth of 1370 m. This is 3.6 km off the shore of Siberia in Asia. Lake Baikal is the world's deepest lake and has a water transparency almost of the quality of deep ocean water. An advantage of this site is that Lake Baikal is covered with up to 1 m of ice in the winter, which provides a stable platform for maintenance carried out during this season. Sea life can interfere with a neutrino detector, as some species give off their own light signals, called bioluminescence, which may trigger the detector. Background light in Lake Baikal is mostly due to bioluminescence and is comparable to the level of light due to radioactive decay seen in the deep ocean.

2.3.3 NESTOR

NESTOR is the Neutrino Extended Submarine Telescope with Oceanographic Research [2], operated by the National Observatory of Athens. This neutrino telescope will be located in the Mediterranean Sea, 15 km south-east off the coast of Peleponnisios, Greece. NESTOR extends to a depth of 3500 m and is Europe's first effort for deep sea high energy neutrino detection. This neutrino telescope will be a tower of 12 hexagonal floors, 32 m in diameter, with vertical intervals of 20 m.

2.3.4 ANTARES

ANTARES stands for Astronomy with a Neutrino Telescope and Abyss environmental REsearch [24] and is located in the Mediterranean Sea. The first prototype for this experiment was deployed in 1999, and in 2006 the first downward going muons were reconstructed. In 2005 the Japan earthquake was detected by ANTARES at 6.2 magnitude. ANTARES has a surface area of 0.1 km^2 with a height of about 350 m. ANTARES will contain 1000 photo multiplier tubes on 12 vertical strings. Strings will be 70 m apart with optical modules spaced 14.5 m on the strings.

2.3.5 AMANDA

AMANDA is the Antarctic Muon And Neutrino Detector Array [3] and has been operational since January 1997. AMANDA is situated at the South Pole in Antarctica. The ice at the South Pole is a large natural volume of uniform material. At the depth the detector is situated at, the medium is dark but still transparent so light signals are easily observable. Building a neutrino telescope under ice allows scientists to walk across the

surface when constructing it which is a huge advantage, as is the absence of sea life inside the detector. There are some disadvantages to building a detector under ice, once the detector is frozen into the ice it is no longer reachable for maintenance. The ice contains dust layers which may lead to scattering of light, however these dust layers have provided an interesting new area of research concerning the geographic evolution of the polar cap. AMANDA is a prototype for a larger detector called IceCube and is contained within the IceCube detector. The AMANDA-II array, an upgraded version of the original AMANDA detector, has been collecting data from February 2000 and has been run in coincidence with IceCube since 2005.

2.3.6 IceCube

IceCube is an international project, and although only one quarter completed, it is already the largest neutrino telescope in the world [1, 15]. IceCube is situated at the South Pole in Antarctica and will have an effective volume of 1 km^3 . Holes are drilled in the ice to a depth of 2.4 km using the Enhanced Hot Water Drill (EHWD) which is a high velocity stream of hot water directed by gravity. IceCube will contain 70 vertical strings lowered into the ice with 60 digital optical modules on each string. With this configuration there will be 17 m vertically between each digital optical module and 125 m between each string with a minimum of 4200 digital optical modules in total. The successful deployment and operation of these digital optical modules was tested on string 14 in the prototype for IceCube, AMANDA, and is now being used in the construction of IceCube. These digital optical modules are self contained data acquisition platforms with a high voltage power supply, an analog transient waveform digitiser, LED flashers and a photomultiplier tube housed in a transparent pressure sphere. Information is transferred to the surface data acquisition system via twisted pair electrical cable. Currently IceCube has 22 strings under the ice and there will be another 14 strings deployed under the ice each field season until the telescope is completed. The full IceCube detector is on schedule to be fully constructed and operational by 2011.

The in ice detectors of IceCube are complemented by a surface air shower array called IceTop. Each IceTop station is situated above a string site and will consist of two large tanks of ice containing 4 optical modules. The size of these tanks is 1 m^2 in area and they are separated by 10 m. The IceTop array can be used for calibration and the exclusion of background noise from atmospheric neutrinos and air showers. IceTop, combined with IceCube, will cover an energy spectrum that includes two distinct groups of cosmic rays. Lighter cosmic rays such as protons and the heavier cosmic rays such as nuclei.

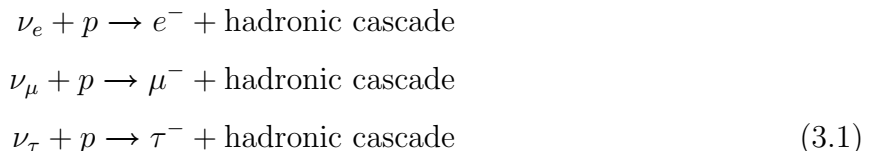
Chapter 3

Physics of Neutrino Detection

This chapter describes the electron, muon and tau neutrino interactions and the signals that are observed from these interactions. As mentioned earlier these neutrinos are detected through observation of Cerenkov radiation. The production of Cerenkov optical photons and the distributions that are expected is discussed and calculations of the number of Cerenkov optical photons produced per unit track length are shown for muons and taus.

3.1 Leptonic interactions

There are three flavours of leptons, each flavour consists of a doublet of a charged lepton and a neutrino. Each of these neutrino flavours can interact with a proton in a detector, producing its associated charged lepton [19]. The direction of this charged lepton is close to the initial direction of the incoming neutrino [26]. In each of these neutrino interactions a hadronic cascade is produced which may be detectable. In the following sections each interaction will be discussed in turn. The three neutrino interactions producing their associated charged lepton and a hadronic cascade are shown in figure 3.1.



The muon produced in the second interaction can be detected by IceCube. There are three factors that detract from the accuracy of reconstructing the direction of travel of a muon [26]. The first is the scattering angle of the neutrino and proton interaction. This

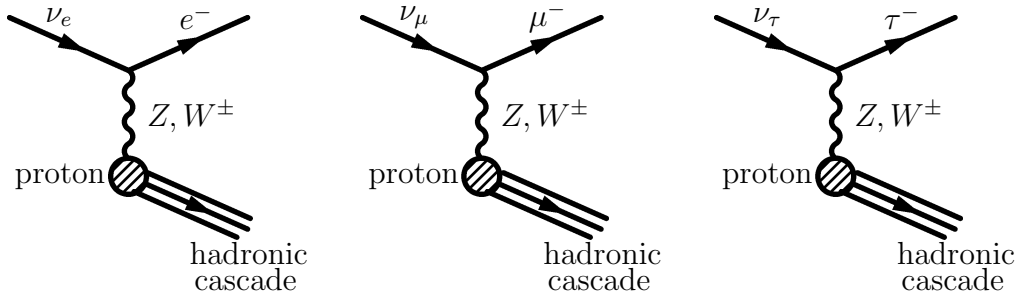


Figure 3.1: Electron, muon and tau neutrino interaction with a proton in a detector.

angle is very small, on the order of one degree. There is a very small contribution from deflection by the earth's magnetic field. This contribution is on the order of less than one tenth of a degree. During its propagation the muon may also be deflected by interactions such as multiple scattering. This appears if as the muon is wobbling as it travels through the detector. Understanding these processes and how they influence the light output we expect is essential to interpreting the data in a meaningful way.

3.1.1 The electron neutrino interaction

The electron produced in an electron neutrino interaction will cause an electromagnetic cascade, producing electrons, positrons and photons. A 100 TeV electromagnetic cascade will be approximately 8.5 m long [8]. The primary interactions in this cascade are Bremsstrahlung and pair production and are shown in figure 3.2. The total track length of the cascade is defined as the sum of the length of the tracks of all these particles, and can be deduced from the amount of Cerenkov light observed. This total track length is proportional to the energy of the cascade, and therefore the energy that initially went into the electron produced in the neutrino interaction. This energy plus the energy of the hadronic cascade is the energy of the incoming electron neutrino.

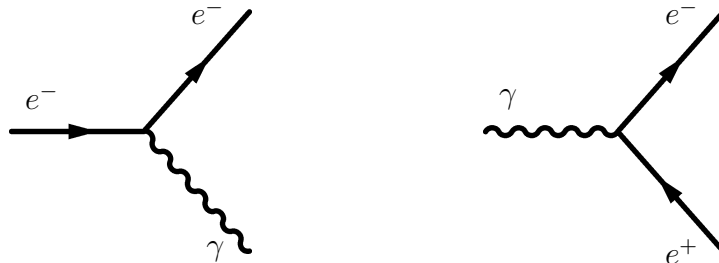


Figure 3.2: Bremsstrahlung and pair production in an electromagnetic cascade.

Each of the electrons and positrons produced will emit their own Cerenkov light since they are charged particles travelling faster than the local speed of light in the medium. The

multiple Cerenkov cones mean the light produced from an electron neutrino interaction is smeared out and has the appearance of a diffuse ring of light [26]. The Cerenkov angle is still prominent but less well defined because there exists a large number of photons emitted in directions away from the Cerenkov angle. A cascade that is not extremely high energy appears as a point source of light in the detector.

3.1.2 The muon neutrino interaction

Muons have a larger mass than electrons and so undergo fewer multiple scattering's and emit fewer Bremsstrahlung photons. For this reason muons are able to travel long distances in ice. A 1 TeV muon will travel approximately 3 km through ice [8]. The long muon tracks makes their Cerenkov signal easier to distinguish from noise. The fewer particles being produced along the muons track means there are not as many charged particles producing Cerenkov cones as in the electron case. The Cerenkov light is not as smeared out and the Cerenkov angle is sharper than in the electron case.

The interactions a muon undergoes as it travels across the detector are Bremsstrahlung, pair production, multiple scattering, ionization and muon capture at rest. If these processes have large energy transfers they may give rise to local cascades. The Feynman diagram for a muon undergoing Bremsstrahlung is in figure 3.3.

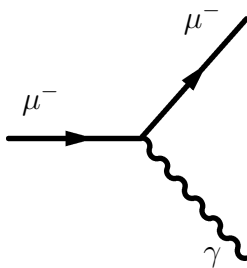


Figure 3.3: Bremsstrahlung in a hadronic cascade.

Multiple scattering occurs as the muon scatters off particles in the surrounding medium, and ionization occurs as a muon loses energy to the surrounding medium. All of these processes, with the exception of muon capture at rest, are a means whereby a muon loses kinetic energy. Muon capture at rest occurs when a muon has lost most of its kinetic energy and slows to almost a stop. Due to its negative charge a muon is then captured by an atom in the surrounding medium. The muon in this case behaves like an electron in the atom that has captured it. This process does not occur for anti-muons which are positively charged.

3.1.3 The tau neutrino interaction

Tau, produced in tau neutrino interactions, is the heaviest lepton and has a short lifetime. This means a tau will decay fast producing a secondary hadronic cascade. This process is discussed more in chapter 5 where a table showing the decay modes and branching ratios is given. An example of a Feynman diagram of tau decay is shown in figure 3.4. The details of the interaction at the vertex where a W^\pm boson is exchanged are omitted. In this case the decay product is a pion, this decay mode has a branching ratio of 11%.

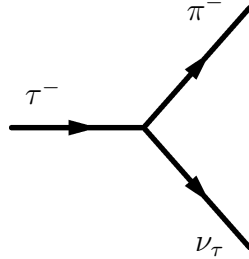


Figure 3.4: Example of tau decay.

These two hadronic cascades from the tau neutrino interaction and the tau decay have been coined the ‘double bang’ since there are two separate bursts of light in the detector [15]. This is observable provided the tau travels far enough away from the neutrino interaction site before it decays for the light from the secondary cascade to be distinct. If the tau neutrino interaction and first hadronic cascade occur outside the detector area, the resulting tau track and hadronic cascade from the tau decay has been coined the ‘lollipop’ [15].

3.2 Hadronic cascades

The hadronic cascade part of the interaction is produced from a Z or W^\pm exchange with a proton in the medium. The proton is split up into its quark constituents which produces hadrons by fragmentation. The energy transferred to the hadronic cascade is around 20 % of the neutrino’s incoming energy as it interacted with the proton. There are however large fluctuations in this interaction so in some cases the majority of the energy of the incoming neutrino can be transferred into the hadronic cascade. The spread of a hadronic cascade is usually broader than electromagnetic cascades with a larger spread in particle tracks. Although the light is still roughly the shape of a spherical ball, this is less homogeneous with not all particle tracks pointing toward the centre of the cascade. The Cerenkov light signal from a hadronic cascade is usually somewhat dimmer than that

from an electromagnetic cascade [26].

3.3 Cerenkov radiation

Cerenkov radiation occurs when any charged particle travels faster than the local speed of light in a dispersive medium [6]. It can be shown that Cerenkov radiation will be produced at a distinct angle relative to the path of the particle, and appears as a cone of light [16, 23]. This angle is dependent on the medium. The local speed of light in a medium is denoted c_n , and is given by $c_n = \frac{c}{n}$ where c is the absolute speed of light in vacuum, and n is the refractive index of the medium. The refractive index is a constant dependent only on the wavelength of the photon travelling through the medium. In ice the refractive index is $n = 1.31$ for visible wavelengths. This means that the local speed of light in ice is approximately 0.76 times that of the absolute speed of light in vacuum.

$$c_n = \frac{c}{n} = 2.288492046 \times 10^8 \text{ ms}^{-1} \quad (3.2)$$

The refractive index gives the Cerenkov angle from the relationship $\cos(\theta_C) = \frac{1}{n\beta}$. Here β is the usual $\frac{v}{c}$ and can be set to one since particles are travelling near the absolute speed of light in vacuum. This gives the expected Cerenkov angle in ice to be

$$\theta_C = \cos^{-1} \left(\frac{1}{n\beta} \right) = 40.24^\circ \quad (3.3)$$

As the relativistic particles speed decreases the number of photons produced drops off, and the photons are emitted with a higher momentum. The Cerenkov angle also decreases. When the particles velocity drops below the local speed of light in the medium Cerenkov radiation is no longer emitted. The energy loss due to Cerenkov radiation is small compared to the energy loss due to ionization. Once Cerenkov photons have been emitted they undergo one of two processes, Rayleigh scattering or optical absorption.

3.4 Optical photons

The expected number of optical photons per track length may be calculated as follows. The Cerenkov radiation per unit distance along the path of the particle is given by [5]

$$\left(\frac{dE}{dx} \right)_{\text{rad}} = \frac{(ze)^2}{c^2} \int_{\epsilon(\omega) \geq \frac{1}{\beta^2}} \left(1 - \frac{1}{\beta^2 \epsilon(\omega)} \right) \omega d\omega \quad (3.4)$$

where ze is the charge of the particle, $\epsilon(\omega)$ is the dielectric constant of the medium and ω is the particles frequency. This integral shows that the radiation is not emitted uniformly,

it is emitted in bands where $\epsilon(\omega) \geq \beta^{-2}$ holds. This condition means the speed of the particle must be larger than the phase velocity of the electromagnetic field to obtain Cerenkov radiation. In other words the particle must be travelling faster than the local speed of light. With some working this energy loss equation gives the number of optical photons that are expected to be emitted due to Cerenkov radiation,

$$\frac{dN}{dx} = 370z^2 \left[E_{\max} - E_{\min} - \frac{1}{\beta^2} \int_{E_{\min}}^{E_{\max}} \frac{1}{n^2} dE \right] \quad (3.5)$$

Here E_{\max} and E_{\min} are the maximum and minimum energies observed by the detector. Neutrino detectors are sensitive to optical wavelengths and for simulation reasons this energy window is 2.034 eV to 4.136 eV which corresponds to $300 \text{ nm} \leq \lambda \leq 610 \text{ nm}$. This equation now becomes

$$\frac{dN}{dx} = 370 \left(2.102 - \frac{1}{n^2\beta^2} \right) \quad (3.6)$$

where z has been set to one and n is treated as a constant over optical wavelengths.

We have substituted values for n and β into this equation to calculate the number of photons per cm of track length. This is shown for muons and taus at 10, 20, 30, 40 and 50 GeV, but can be found for any particle with any energy above the Cerenkov threshold. Using the energies and masses β has been calculated using the γ -factor of the particles. This gives the following results shown in table 3.1. In the calculations leading

Energy	Photons per cm for a muon	Photons per cm for a tau
10 GeV	562.111	557.112
20 GeV	562.129	560.690
30 GeV	562.132	561.459
40 GeV	562.133	561.744
50 GeV	562.133	561.881

Table 3.1: Optical photons produced per centimetre of track length from Cerenkov radiation.

to the numbers in table 3.1, β is assumed constant throughout the particles travel. This is a reasonable assumption since the value for β drops off sharply as Cerenkov radiation ceases. If β is assumed to be one, the number of photons per unit track length reaches a maximum. We have calculated this maximum number of photons per unit of track length to be

$$\left(\frac{dN}{dx} \right)_{\max} = 562.135 \text{ photons cm}^{-1} \quad (3.7)$$

Chapter 4

Simulation Programs

This chapter contains a short description of the simulation programs, Pythia and GEANT. These simulation programs are commonly used high energy physics and we use them in this work.

4.1 Pythia – The event generation

Pythia is an event generator for high energy particle physics. The interactions are broken down into many separate components and each is handled with a high level of accuracy. The output has averaged behaviour and also contains fluctuations. Monte Carlo techniques are used so the final result is non deterministic. The version of Pythia used throughout this work is Pythia 6.2 [22], which is written using FORTRAN 77 [7].

The Pythia event generator includes simulation of initial and final state radiation, multiple interaction among beam jets and fragmentation, all of which are enabled in our simulations. There is also a High Energy Physics (HEP) subroutine available that produces an event record in a Monte Carlo independent format.

4.1.1 Initial and final state radiation

Initial and final state radiation are higher order loop corrections. Initial state radiation occurs when an initial particle emits a photon that is then absorbed by a final particle. Final state radiation is the timelike version of this and occurs when an final particle emits a photon that is then absorbed by an initial particle.

4.1.2 Multiple interaction among beam jets

Every incoming particle may leave behind a beam remnant which has properties of flavour and colour dependent on the particle. This beam remnant may undergo multiple interactions.

4.1.3 Fragmentation

Fragmentation is modeled by the Lund string scheme. This model is an iterative approach where an initial quark may create a new quark pair forming a meson and one quark left over. This quark may also create a new quark pair and another quark left over and so on. This model uses the relative probabilities for quark-anti quark formation and the relative probabilities that a given quark pair forms a specific meson. In the Lund string scheme the concept of quantum tunnelling is used to form quark - anti quark pairs which leads to string break ups.

4.1.4 HEP subroutine

The subroutine produces output from Pythia in a format that may be read by the GEANT interface. This interface requires specific information about each particle that is fed into the GEANT simulation.

4.2 GEANT 4.8 – The event simulation

GEANT is a program that is used to simulate the passage of particles through matter. This program is written in C++ and uses its object orientated framework to deal with the interactions of particles with matter over a large energy range. The version of GEANT used throughout the following work is GEANT 4.8 [5, 11].

4.2.1 Hadronic and Cerenkov processes

The hadronic processes are modelled using the QGSP which is an ‘educated guess physics list’ contained within GEANT. This uses theory driven modelling for reactions of pions, kaons and nucleons.

The production of optical photons through the Cerenkov process was added to the GEANT framework. The source code that includes this additional physics is shown in

appendix A.

4.2.2 Detector Construction

GEANT provides code for generating particular detector constructions. The code does not simulate neutrino detectors so this code must be altered considerably in order to accurately simulate neutrino telescopes. We have done this for the neutrino telescope IceCube. A large block of ice was defined by creating a three dimensional volume of ice. The volume is then given the properties of refractive index and absorption for each wavelength of light that propagates through the ice. Values for the refractive index depend only on the phase velocity in the medium [18] and are listed in the tables in the photonics package [20]. The unique code we have used to simulate the IceCube detector construction is shown in appendix B.

Chapter 5

Detection of the Tau Lepton

Tau neutrino interaction and tau lepton detection are studied in this chapter. This is carried out by running simulations of tau processes. These results are compared with similar simulations run for muons. The number of Cerenkov optical photons produced per centimetre of track length in the simulations are compared with theoretical values.

5.1 Tau and the tau neutrino

Many simulations have been carried out with the Cerenkov distribution studied for the electron and muon neutrino interactions. The tau neutrino has not been studied in as much detail, as it has a smaller matter interaction cross section and earlier neutrino detectors have smaller effective volume making the detection of tau neutrinos interactions difficult. The mass of the tau is 1777 MeV and has a lifetime of 2.96×10^{-13} seconds [12]. In comparison to the other leptons this lifetime is very short; the muon has a lifetime of 2.2×10^{-6} seconds and the electron is stable so does not decay. It has been hypothesised that the Cerenkov radiation from tau should look similar to that from a muon but with a scaling factor of approximately one tenth the brightness. Simulations may be run to study the Cerenkov distribution for muons and tau to in order to confirm this hypotheses.

It is hoped that the completed IceCube will have a large enough effective area to detect tau. There have been suggestions concerning the light output expected if a tau neutrino entered the detector. These include the ‘double bang’ and the ‘lollipop’ [15]. However, simulations must be run to ascertain if this is what would actually be observed and what the Cerenkov light output would look like particularly in comparison to that of the muon so that they might be distinguished. GEANT 4.8 has the framework that is necessary to run these types of simulations.

5.2 Processes

There are five processes that we will consider which a tau may undergo when travelling through the detector. These are decay, multiple scattering, ionization, Bremsstrahlung, and pair production. These processes are the same as those present for muon simulations with the exception of muon capture at rest.

5.2.1 Decay

Basis decay modes and branching ratios for tau are shown in table 5.1. Decay modes for a positive tau are the charge conjugates of these modes. The process of decay is already built into GEANT 4.8 [5]. With the usual $\gamma = \frac{1}{\sqrt{1-\beta^2}}$ and $\beta = \frac{v}{c}$ the mean free path, λ , for a particle is calculated using

$$\lambda = \gamma\beta c\tau \quad (5.1)$$

where c is the absolute speed of light in vacuum and τ is the decay lifetime of the particle in its rest frame. From the momentum of the particle, γ and β can be calculated at the beginning of each step in the program. The decay mode is selected and the branching ratio is known for each decay mode. The decay is simulated using $V - A$ theory. The energies of the resulting neutrinos after a decay are calculated using energy and momentum conservation.

5.2.2 Multiple scattering

The Lewis theory is used to simulate multiple scattering of charged particles [5]. This simulates scattering after a given step in the program and calculates the path length corrections and the lateral displacement of the particle. Multiple scattering is a similar process for all particles and can be added to the GEANT 4.8 simulation for tau using the existing framework.

5.2.3 Ionization

Relativistic heavy charged particles travelling through media always lose energy. Energy loss is due to ionization and atomic excitation as the particle interacts with electrons in the medium. Particles lose energy per unit distance travelled according to the Bethe-Bloch equation [12].

$$\frac{-dE}{dx} = 4\pi N_A r_e^2 m_e c^2 z^2 \frac{Z}{A} \frac{1}{\beta^2} \left[\frac{1}{2} \ln \left(\frac{2m_e c^2 \beta^2 \gamma^2 T_{\max}}{I^2} \right) - \beta^2 - \frac{\delta}{2} \right] \quad (5.2)$$

Decay type	Decay mode	Branching ratio (%)
One charged particle	$\tau^- \rightarrow \mu^- + \bar{\nu}_\mu + \nu_\tau$	17.37
	$\tau^- \rightarrow e^- + \bar{\nu}_e + \nu_\tau$	17.84
	$\tau^- \rightarrow \pi^- + \nu_\tau$	11.06
	$\tau^- \rightarrow K^- + \nu_\tau$	6.86×10^{-3}
	$\tau^- \rightarrow \pi^- + \pi^0 + \nu_\tau$	25.41
	$\tau^- \rightarrow K^- + \pi^0 + \nu_\tau$	4.50×10^{-3}
	$\tau^- \rightarrow \pi^- + 2\pi^0 + \nu_\tau$	9.17
	$\tau^- \rightarrow K^- + 2\pi^0 + \nu_\tau$	5.8×10^{-4}
	$\tau^- \rightarrow \pi^- + 3\pi^0 + \nu_\tau$	1.08
	$\tau^- \rightarrow K^- + 3\pi^0 + \nu_\tau$	3.7×10^{-4}
	$\tau^- \rightarrow (\pi^- \text{ or } K^-) + 4\pi^0 + \nu_\tau$	1.0×10^{-3}
Modes with K^0 's	$\tau^- \rightarrow \pi^- + \bar{K}^0 + \nu_\tau$	8.9×10^{-3}
	$\tau^- \rightarrow K^- + K^0 + \nu_\tau$	1.54×10^{-3}
	$\tau^- \rightarrow \pi^- + \bar{K}^0 + \pi^0 + \nu_\tau$	3.7×10^{-3}
	$\tau^- \rightarrow K^- + K^0 + \pi^0 + \nu_\tau$	1.55×10^{-3}
	$\tau^- \rightarrow \pi^- + 2K_S^0 + \nu_\tau$	2.4×10^{-4}
	$\tau^- \rightarrow \pi^- + K_S^0 + K_L^0 + \nu_\tau$	1.10×10^{-3}
Three charged particles	$\tau^- \rightarrow \pi^+ + 2\pi^- + \nu_\tau$	9.17
	$\tau^- \rightarrow \pi^+ + 2\pi^- + \pi^0 + \nu_\tau$	2.51
	$\tau^- \rightarrow 2(\pi^- \text{ or } K^-) + (\pi^+ \text{ or } K^+) + 2\pi^0 + \nu_\tau$	1.1×10^{-3}
	$\tau^- \rightarrow 2(\pi^- \text{ or } K^-) + (\pi^+ \text{ or } K^+) + 3\pi^0 + \nu_\tau$	2.3×10^{-4}
	$\tau^- \rightarrow K^- + \pi^+ + \pi^- + \nu_\tau$	2.8×10^{-3}
	$\tau^- \rightarrow K^- + \pi^+ + \pi^- + \pi^0 + \nu_\tau$	6.4×10^{-4}
	$\tau^- \rightarrow K^- + K^+ + \pi^- + \nu_\tau$	1.6×10^{-3}
	$\tau^- \rightarrow K^- + K^+ + \pi^- + \pi^0 + \nu_\tau$	4.0×10^{-4}
Five charged particles	$\tau^- \rightarrow 3(\pi^- \text{ or } K^-) + 2(\pi^+ \text{ or } K^+) + \nu_\tau$	8.2×10^{-4}
	$\tau^- \rightarrow 3(\pi^- \text{ or } K^-) + 2(\pi^+ \text{ or } K^+) + \pi^0 + \nu_\tau$	1.81×10^{-4}
Other modes	$\tau^- \rightarrow \eta + \pi^- + \pi^0 + \nu_\tau$	1.74×10^{-3}
	$\tau^- \rightarrow \eta + K^- + \nu_\tau$	2.7×10^{-4}
	$\tau^- \rightarrow (\pi^- \text{ or } K^-) + \omega + \nu_\tau$	1.94
	$\tau^- \rightarrow (\pi^- \text{ or } K^-) + \omega + \pi^0 + \nu_\tau$	4.3×10^{-3}

Table 5.1: Basis decay modes and branching ratios for tau minus [12].

Here the constants are N_A , Avagadro's number, r_e , the classical electron radius and m_e , the electron mass. The other terms concern properties of the particle and the surrounding medium. These are z , the charge on the incident particle, Z , the atomic number of the absorber, A , the atomic mass of the absorber, I , the mean excitation energy of the target and δ , the density effect correction to the ionizing energy loss. T_{\max} is the maximum kinetic energy that can be imparted to a free electron in a single collision. For low energies ($\beta \ll 1$) energy loss decreases as $\frac{1}{v^2}$ and reaches a minimum at $E = 3mc^2$. For relativistic particles ($\beta \approx 1$), the logarithmic term in the Bethe-Bloch equation becomes dominant and energy loss increases logarithmically due to these relativistic effects. Slower moving particles lose energy more quickly since they have more time to interact with the electrons in the surrounding medium. The minimum ionizing particle point (MIP) is at about the same momentum for different materials, 30 GeV to 35 GeV as Z goes from 7 to 100, in the case of neutrino detectors built in ice the average molar mass of the medium is just above 18. There is a slow decrease in rate of energy loss with increasing Z . The Bethe-Bloch equation has some limits, corrections have to be made at very low energies and very high energies where radiative effects begin to be important. These limits depend on the effective number of the absorber, Z , and the mass of the travelling particle. Most relativistic particles have an energy loss close to the minimum and are called minimum ionizing particles (MIPs). The most probable energy loss in a detector is actually below the mean given by the Bethe-Bloch equation. The equation may be integrated to find the 'continuous slowing down approximation'.

There is no process in GEANT 4.8 to simulate ionization for tau. There are three types of ionization in GEANT 4.8 [5], one for electrons, one for muons and one for charged hadrons. The process for electrons is very different to the other two processes since the Bethe-Bloch equation can not be used. The energy loss for muons and charged hadrons are very similar to each other. This process provides a continuous energy loss due to ionization and simulates delta rays produced by the particle. The simulation of ionization for muons and charged hadrons uses T_{\max} , the maximum energy transferable to a free electron in a single collision which is given by

$$T_{\max} = \frac{2mc^2(\gamma^2 - 1)}{1 + 2\gamma\left(\frac{m}{M}\right) + \left(\frac{m}{M}\right)^2}, \quad (5.3)$$

where m is the mass of the electron and M is the mass of the particle. In the hadronic case energy loss tables are only calculated for protons and the energy loss for heavy charged particles is calculated from the scaled kinetic energy

$$T_{\text{scaled}} = \frac{M_{\text{proton}}}{M_{\text{particle}}} T, \quad (5.4)$$

where T is the kinetic energy of the particle and M_{proton} and M_{particle} are the masses of the proton and particle respectively. The difference in the T_{max} value for different charged particles in this method is neglected. This is not acceptable in the case of electrons and muons. This method works for tau since the mass of the tau, 1777 MeV is in the middle of the range of masses for the charged hadrons. These ranges are 938.3 – 2281 MeV for baryons and 139.6 – 9460.4 MeV for mesons. It is this model of ionization that is added to GEANT 4.8 for tau simulations.

5.2.4 Bremsstrahlung and pair production

Both Bremsstrahlung and pair production are not available for tau in GEANT 4.8. Due to the large mass of tau, its Coulomb field does not influence its trajectory as strongly as lower mass charged particles. Tau then undergoes less multiple scattering as it travels across a detector. This results in fewer Bremsstrahlung photons emitted and fewer instances of pair production so these processes are safe to ignore.

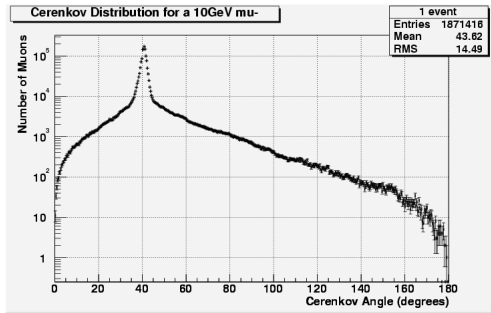
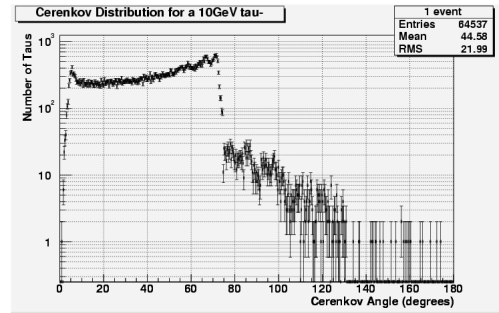
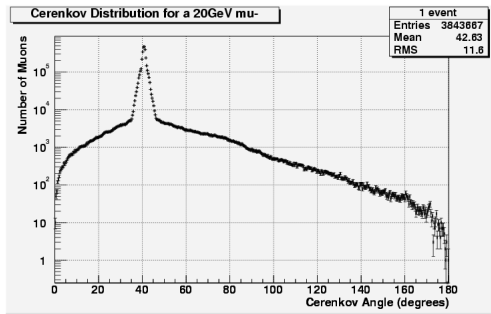
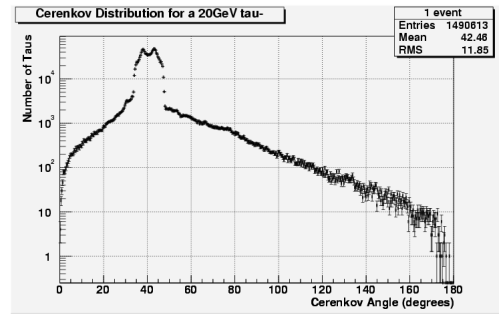
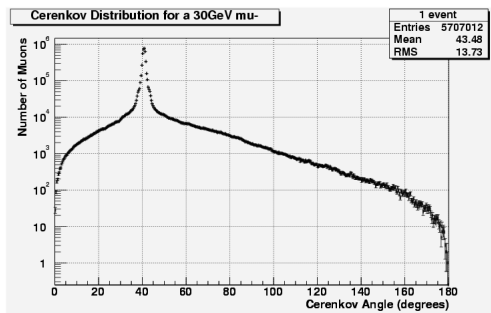
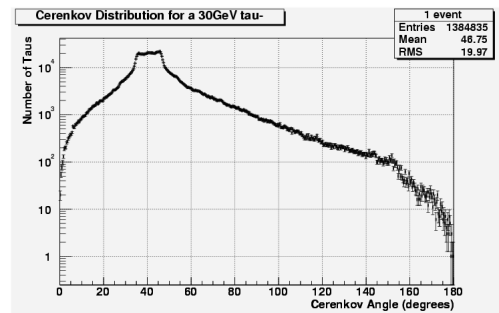
5.3 Cerenkov radiation from muons and taus

The simulations we have run calculate and write out the momentum component along the direction of travel of the muon or tau for every optical photon that is produced. This direction is along the x -axis and the momentum component is denoted p_x . The Cerenkov distribution is plotted using the equation

$$\cos^{-1}(p_x) \frac{180}{3.14}, \quad \text{with a weighting of } \frac{1}{\sin(\cos^{-1}(p_x))} \quad (5.5)$$

This equation transforms the x -components of the momentum into the polar angular Cerenkov distribution and the weighting transforms it to a solid angle distribution [26].

Results of our simulations carried out for both muons and taus are shown in figures 5.1 to 5.10. These simulations range from 10 GeV to 50 GeV for an interaction in ice. Many simulations have been carried out and the Cerenkov distributions we show represent an average of the results. Large fluctuations occurred in some of the simulations. In simulations the process of muon capture at rest can be turned off. Many other studies chose this option because it is the default in GEANT. We include it since this process will always occur in reality. We found that if muon capture at rest is turned off the track length of the muon is longer and so slightly more optical photons are produced. This should be taken into account if a comparison of studies is carried out.

Figure 5.1: Cerenkov angle for 10 GeV μ^- .Figure 5.2: Cerenkov angle for 10 GeV τ^- .Figure 5.3: Cerenkov angle for 20 GeV μ^- .Figure 5.4: Cerenkov angle for 20 GeV τ^- .Figure 5.5: Cerenkov angle for 30 GeV μ^- .Figure 5.6: Cerenkov angle for 30 GeV τ^- .

The Cerenkov angles for the muon angular distributions from the simulations from 10 – 50 GeV are all around 40 degrees. The Cerenkov angles in the case for tau are not so clear. This is because there is a double peak in the angular distribution. For each energy studied the tau decayed into another particle. At the energies where the mean value for the Cerenkov angle is near 40 degrees the particle to which the tau decayed

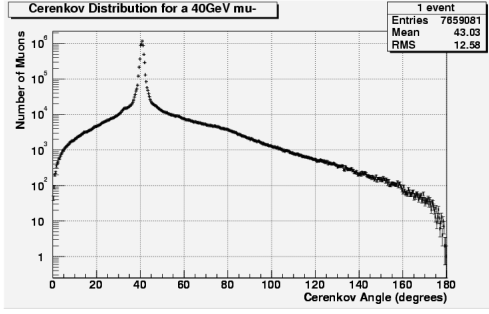


Figure 5.7: Cerenkov angle for 40 GeV μ^- .

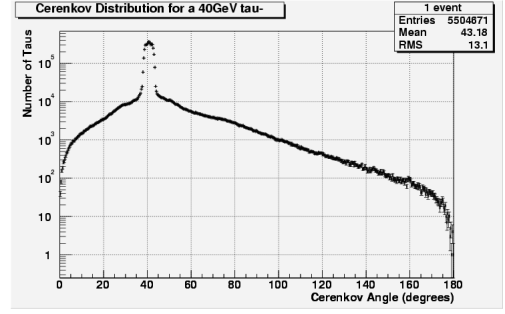


Figure 5.8: Cerenkov angle for 40 GeV τ^- .

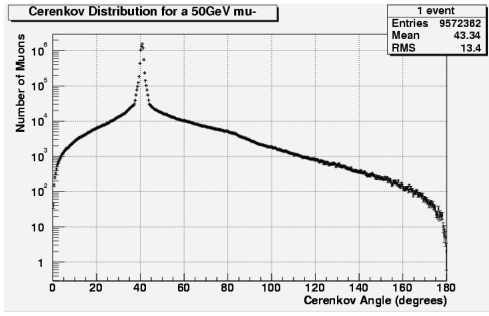


Figure 5.9: Cerenkov angle for 50 GeV μ^- .

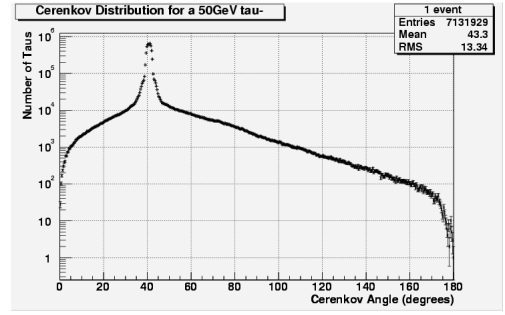


Figure 5.10: Cerenkov angle for 50 GeV τ^- .

approximately follows the same trajectory as the original tau. For the energies where the spacing between peaks is large, in particular the 10 GeV case, the momentum direction of the decay product was rather different from the original tau trajectory. It is because of tau decay that, unlike the electron and the muon, the Cerenkov distribution for tau is not a generic signal. For each of the simulation examples shown in figures 5.2, 5.4, 5.6, 5.8 and 5.10 the decays were studied in more detail. They are listed below.

$$\tau^- \rightarrow \pi^- + \nu_\tau \quad (\text{Fig. 5.2})$$

$$\tau^- \rightarrow \pi^- + \nu_\tau \quad (\text{Fig. 5.4})$$

$$\tau^- \rightarrow e^- + \bar{\nu}_e + \nu_\tau \quad (\text{Fig. 5.6})$$

$$\tau^- \rightarrow \pi^- + \pi^0 + \nu_\tau \quad (\text{Fig. 5.8})$$

$$\tau^- \rightarrow \mu^- + \bar{\nu}_\mu + \nu_\tau \quad (\text{Fig. 5.10}) \quad (5.6)$$

At each energy tau may undergo any decay mode shown in table 5.1. These five decays that occurred in these simulations are some of the decay modes that have the highest

branching ratios, which is a result that we expect.

Table 5.2 shows a comparison of our simulated number of photons produced per cm of track length compared to our calculated values, shown in table 3.1. The photons per centimetre for the simulated values are obtained by dividing the total number of photons for each energy by the total track length for that energy. This comparison is only shown for muons since tau decays. The simulated values may be an underestimation as the track length is obtained for only the primary particles trajectory, the extra track length from other particles produced in minor cascades along its path are neglected.

Energy	Simulated number of photons per cm	Calculated number of photons per cm
10 GeV	583.101	562.111
20 GeV	413.266	562.129
30 GeV	496.417	562.132
40 GeV	431.430	562.133
50 GeV	467.492	562.133

Table 5.2: Comparison of simulated and calculated number of photons per centimetre of track length for a muon.

5.4 Range expectation for tau

In order to see tau travel further across the detector, the incoming tau neutrino would require very high energy. The distance the particle will travel across the detector given its energy can be calculated using the simple formula $d = vt$ where v is the particle's velocity and t is the particle's decay time in its own rest frame. The particles velocity is close to that of the speed of light in vacuum, $v \approx c$ and the dilated time of travel is given by $t = \gamma\tau$. The γ -factor may be found using the energy formula $E = \gamma mc^2$. Taking time dilation into account, a 10 GeV muon would travel 62,000 m and a 10 GeV tau would travel 0.05 cm.

For tau to travel across a 1,000 m detector an energy of at least 20 PeV would be required. For the light from the hadronic cascade of the tau decaying to be distinguishable from the light of the original neutrino interaction, tau would need to travel only part way across the detector. The energy required for this would still be on the order of 1 PeV. The requirement to observe the predicted 'double bang' or 'lollipop' detection is that the distinguishably of the cascade resulting from the tau neutrino interaction and that

resulting from the original tau decay.

Chapter 6

Long Range Muon Production

In this chapter a study of the production of pions and kaons produced in the hadronic cascade following an electron neutrino interaction is presented. This study involves simulations using the Pythia event generator. The y distribution for the simulations are analysed to verify the results. This study is continued by looking at the possible decay of pions and kaons into muons. The energy of the hadronic cascade dictates the nature of the muons detected in a neutrino telescope. The results from the Pythia simulations are used to ascertain the likelihood of the production of these muons and their energies.

6.1 High energy hadrons

When an electron neutrino interacts with a proton via W^\pm exchange in a medium an outgoing electron and a hadronic cascade are produced. The electron goes on to produce an electromagnetic cascade, undergoing the processes of Bremsstrahlung and pair production. The hadronic cascade is formed from the constituents of the proton. This hadronic cascade typically contains approximately 20 % of the original incoming electron neutrinos energy but due to fluctuations may contain the majority of the incoming neutrino's energy. If the energy of the incoming electron neutrino is high, the hadrons in the cascade may also have very high energy. This hadronic cascade will include pions and kaons whose decay products can be muons. Much of the energy from the pions' and kaons' can be transferred to the muons they decay into, resulting in these muons having very high energy.

Muons with high energy are long range and are detected easily when traversing through a detector [15]. A long range muon detection could be interpreted as the product of a muon neutrino interaction rather than the product of an electron neutrino interaction. It

is for this reason that the production of long range muons arising from the decay of high energy pions and kaons needs to be simulated and studied.

Furthermore, hadronic cascades have spherical, inhomogeneous geometry with particle tracks not pointing to the centre of the cascade [26]. This means that the hadronic cascade contains very little directional information about the original incoming neutrino. These hadronic cascades are very difficult to reconstruct in order to obtain the required directional information, and unreliable compared to the elongated cascades produced by the charged leptons. Long range muons could then be of assistance to this reconstruction process. This is of vital importance since a large motivation for neutrino telescopes is due to the neutrino's ability to point back to its source and provide information about its origins.

6.2 Pion and kaon production from electron neutrino interactions

Our simulations, carried out using Pythia, generate an electron neutrino event via W^\pm exchange with a proton. In the subsequent hadronic cascade there may be two types of pions created [22], the positively charged pion π^+ , the negatively charged pion π^- and the neutral pion π^0 . The rest masses and lifetimes of these particles are as follows:

$$\begin{aligned} m_{\pi^\pm} &= 139.57 \text{ MeV}, & t_{\pi^\pm} &= 2.60 \times 10^{-8} \text{ s} \\ m_{\pi^0} &= 134.98 \text{ MeV}, & t_{\pi^0} &= 0.84 \times 10^{-16} \text{ s}. \end{aligned} \quad (6.1)$$

Using the Pythia event generator, there may be ten types of kaons produced [22]. These are K^+ , K^- , K^0 , \bar{K}^0 , K^{*0} , \bar{K}^{*0} , K^{*+} , K^{*-} , K_S^0 and K_L^0 . K^0 and \bar{K}^0 are electrically neutral and propagate as a mixture, either $(K^0 + \bar{K}^0)$ or $(K^0 - \bar{K}^0)$. These two states have different decay times and this is how K_S^0 and K_L^0 arise. The rest mass and lifetimes of these particles are as follows.

$$\begin{aligned} m_{K^\pm} &= 493.68 \text{ MeV}, & t_{K^\pm} &= 1.24 \times 10^{-8} \text{ s} \\ m_{K^0} &= 497.67 \text{ MeV}, & t_{K_S^0} &= 0.89 \times 10^{-10} \text{ s}, & t_{K_L^0} &= 5.17 \times 10^{-8} \text{ s} \\ m_{K^*} &= 891.66 \text{ MeV} \end{aligned} \quad (6.2)$$

Our simulation was carried out for 10 TeV, 100 TeV, 500 TeV, 1 PeV and 2 PeV incoming electron neutrinos. The number of pions and kaons produced are plotted against their energies. This is done for one event (figures 6.1 to 6.10), one hundred events (figures 6.11 to 6.20) and ten thousand events (figures 6.21 to 6.30).

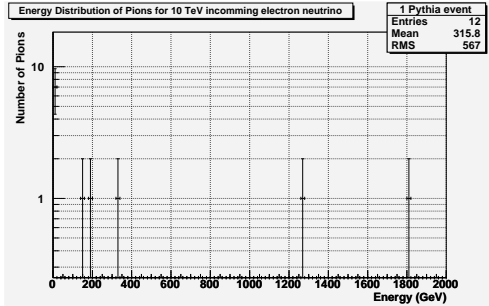


Figure 6.1: Pions produced from one 10 TeV electron neutrino event.

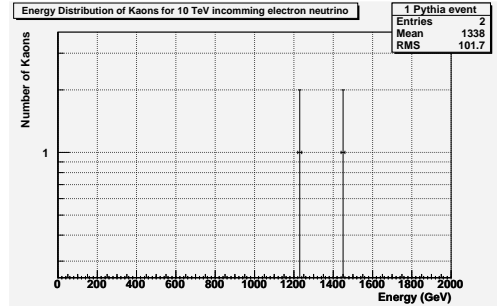


Figure 6.2: Kaons produced from one 10 TeV electron neutrino event.

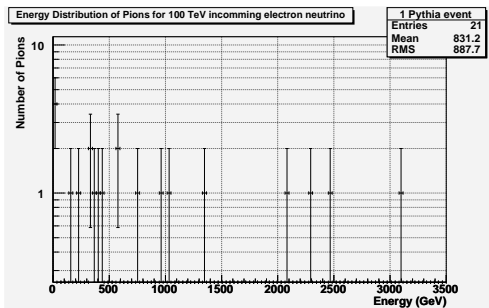


Figure 6.3: Pions produced from one 100 TeV electron neutrino event.

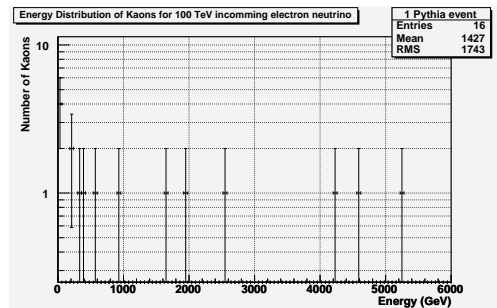


Figure 6.4: Kaons produced from one 100 TeV electron neutrino event.

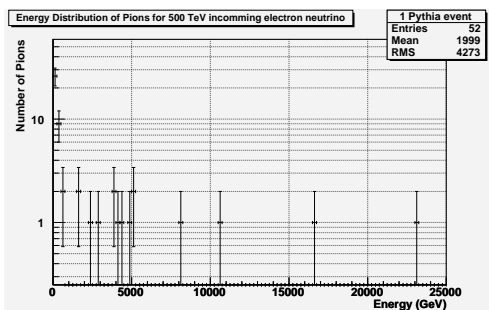


Figure 6.5: Pions produced from one 500 TeV electron neutrino event.

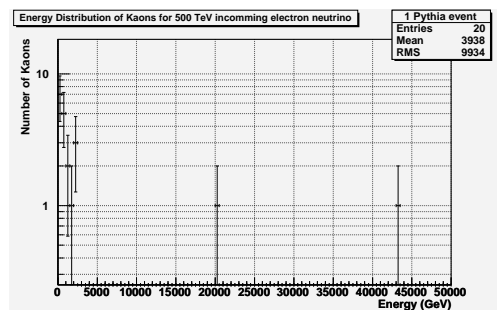


Figure 6.6: Kaons produced from one 500 TeV electron neutrino event.

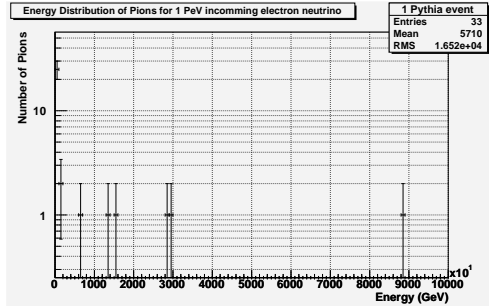


Figure 6.7: Pions produced from one 1 PeV electron neutrino event.

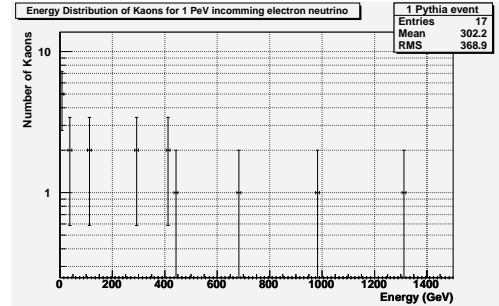


Figure 6.8: Kaons produced from one 1 PeV electron neutrino event.

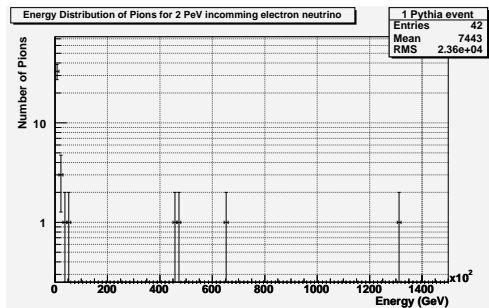


Figure 6.9: Pions produced from one 2 PeV electron neutrino event.

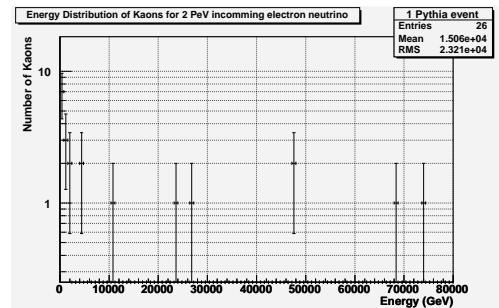


Figure 6.10: Kaons produced from one 2 PeV electron neutrino event.

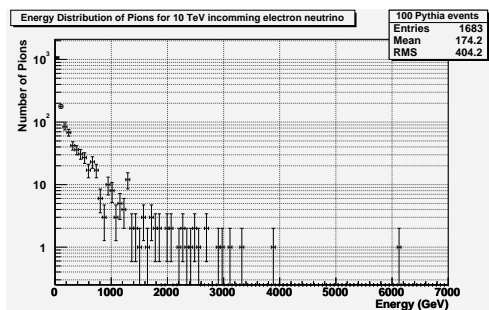


Figure 6.11: Pions produced from one hundred 10 TeV electron neutrino events.

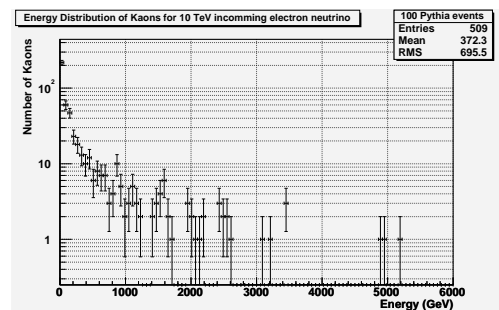


Figure 6.12: Kaons produced from one hundred 10 TeV electron neutrino events.

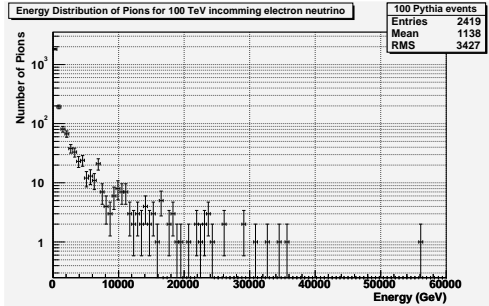


Figure 6.13: Pions produced from one hundred 100 TeV electron neutrino events.

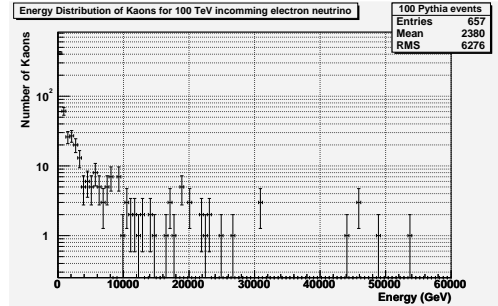


Figure 6.14: Kaons produced from one hundred 100 TeV electron neutrino events.

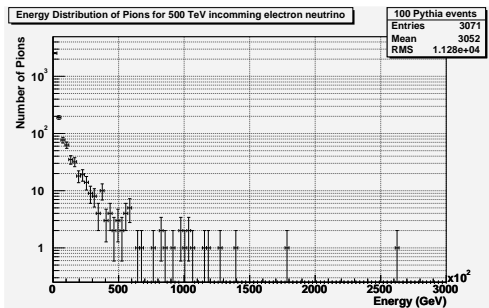


Figure 6.15: Pions produced from one hundred 500 TeV electron neutrino events.

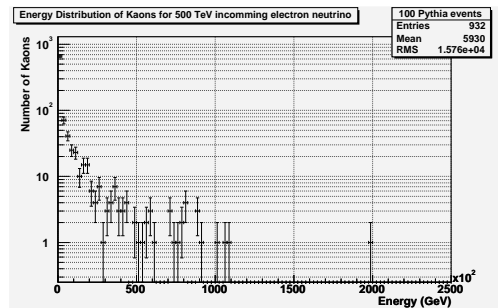


Figure 6.16: Kaons produced from one hundred 500 TeV electron neutrino events.

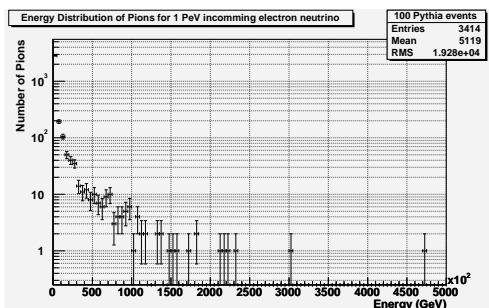


Figure 6.17: Pions produced from one hundred 1 PeV electron neutrino events.

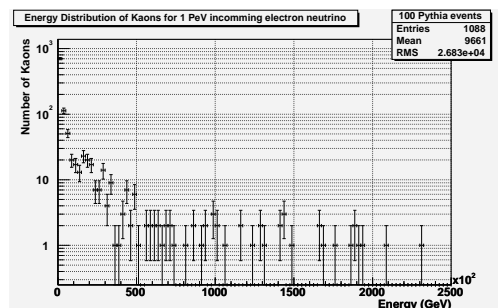


Figure 6.18: Kaons produced from one hundred 1 PeV electron neutrino events.

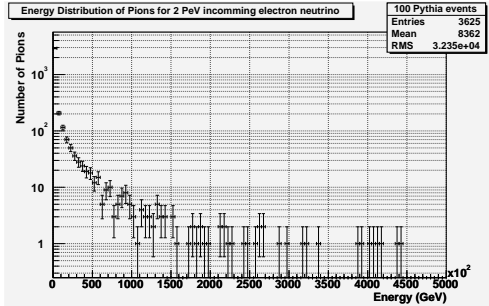


Figure 6.19: Pions produced from one hundred 2 PeV electron neutrino events.

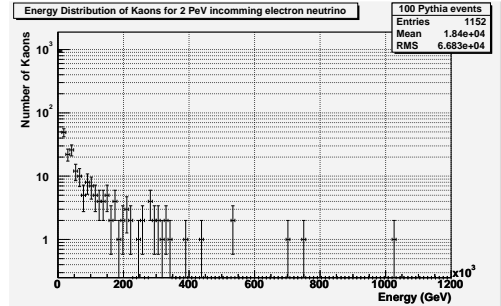


Figure 6.20: Kaons produced from one hundred 2 PeV electron neutrino events.

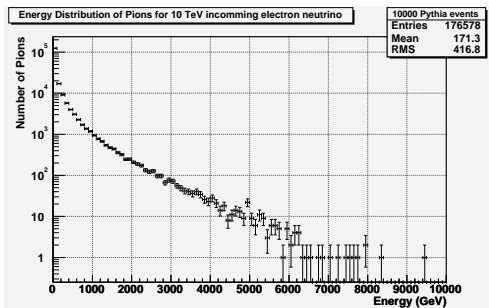


Figure 6.21: Pions produced from ten thousand 10 TeV electron neutrino events.

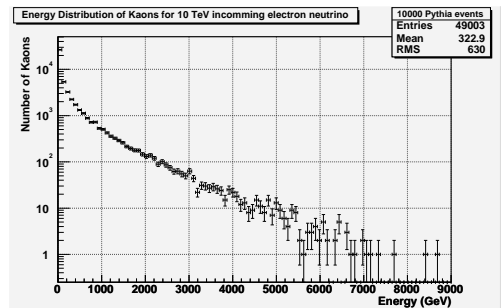


Figure 6.22: Kaons produced from ten thousand 10 TeV electron neutrino events.

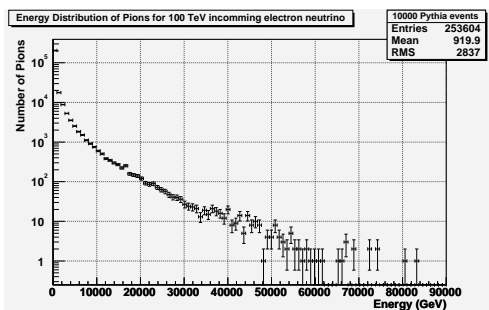


Figure 6.23: Pions produced from ten thousand 100 TeV electron neutrino events.

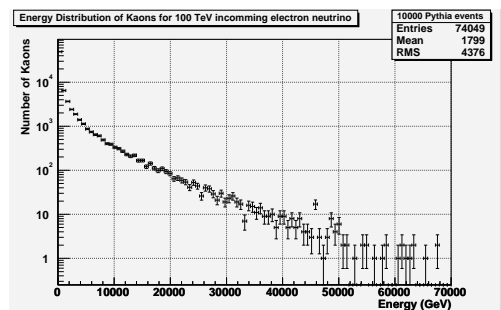


Figure 6.24: Kaons produced from ten thousand 100 TeV electron neutrino events.

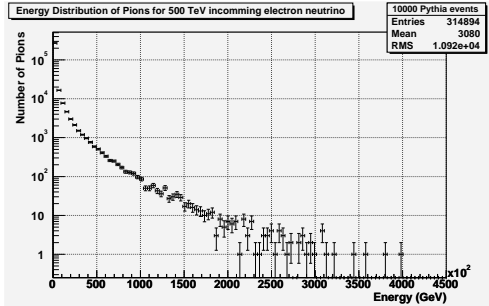


Figure 6.25: Pions produced from ten thousand 500 TeV electron neutrino events.

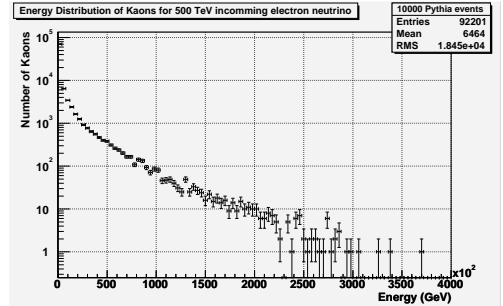


Figure 6.26: Kaons produced from ten thousand 500 TeV electron neutrino events.

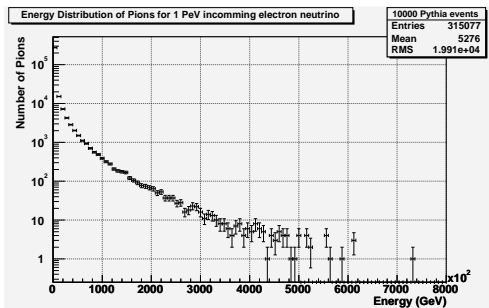


Figure 6.27: Pions produced from ten thousand 1 PeV electron neutrino events.

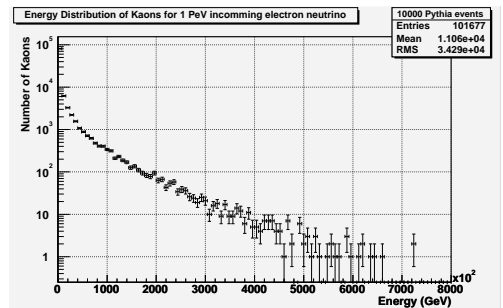


Figure 6.28: Kaons produced from ten thousand 1 PeV electron neutrino events.

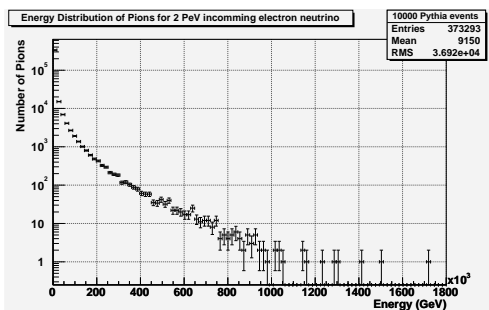


Figure 6.29: Pions produced from ten thousand 2 PeV electron neutrino events.

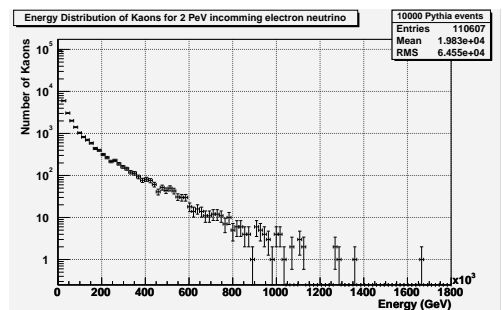


Figure 6.30: Kaons produced from ten thousand 2 PeV electron neutrino events.

Table 6.1 shows the number of particles and the mean energies of the pions and kaons produced for each energy level of our Pythia simulation. The number of pions produced in the hadronic cascade is far greater than the number of kaons produced. In fact the rate of production of pions typically exceeds that of kaons by over three times in these simulations. However, the mean energy of the kaons being produced is greater than that of the pions, typically by about two times the energy of the pions produced. These results tell us that in the hadronic cascade resulting from an electron neutrino interaction there are significant numbers of pions and kaons produced with high energies. We may expect that many of these pions and kaons will decay into muons which may also have very high energies. This, as predicted, will give detectable long range muons in a neutrino telescope. These long range muons may be interpreted as a muon neutrino interaction, and hence are ‘fake’ muon neutrino events. The extent to which this occurs is studied in further detail using GEANT 4.8 subsequently.

	Energy	Number of particles		Mean energy of particles (GeV)	
		Pions	Kaons	Pions	Kaons
1 event	10 TeV	12	2	315.8	1,338
	100 TeV	21	16	831.2	1,427
	500 TeV	52	20	1,999	3,938
	1 PeV	53	17	5,710	302.2
	2 PeV	42	26	7,443	15,060
100 events	10 TeV	1,683	509	174.2	372.3
	100 TeV	2,419	657	1,138	2,380
	500 TeV	3,017	932	3,052	5,930
	1 PeV	3,414	1,088	5,119	9,661
	2 PeV	3,625	1,152	8,362	18,400
10,000 events	10 TeV	176,578	49,003	171.3	322.9
	100 TeV	253,604	74,049	919.9	1,709
	500 TeV	314,894	92,201	3,080	6,464
	1 PeV	315,077	101,677	5,276	11,060
	2 PeV	373,293	110,607	9,150	13,830

Table 6.1: Number of pions and kaons and their mean energy in our Pythia simulations.

6.3 The y distribution

In order to verify that Pythia accurately simulates the electron neutrino interaction and the resulting hadronic cascade we may look at the y distribution [10]. This is the mean inelasticity of the distribution and is given by

$$y = \frac{E_\nu - E_e}{E_\nu} \quad (6.3)$$

where E_ν is the energy of the incoming electron neutrino and E_e is the energy of the outgoing electron. We have looked at the y distribution for 1,000 events over an energy range of 10 GeV to 10^{12} GeV. For each energy there are 1,000 points and these are averaged and compared to the theoretical values calculated by [10]. This comparison is shown in figure 6.31.

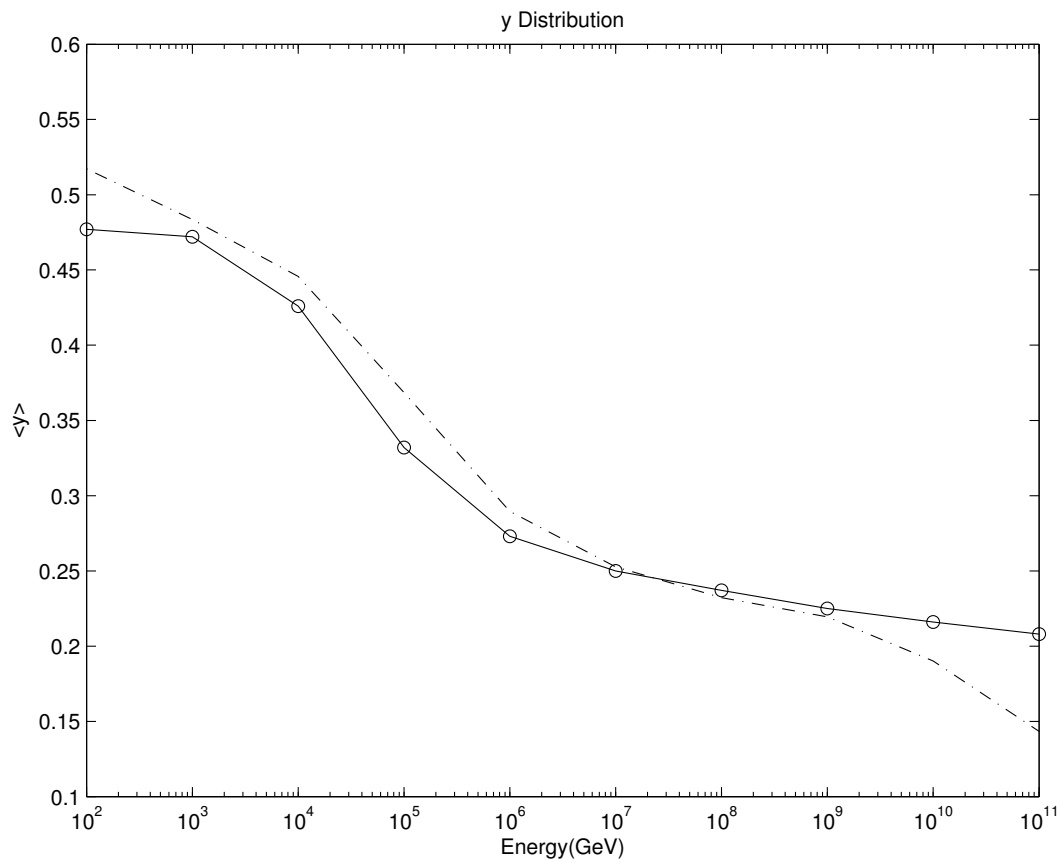


Figure 6.31: Comparison of our simulated y distribution to the theoretical y distribution calculated by Gandhi *et al.* [10].

In figure 6.31 the solid line is the theoretical values and the dashed line shows our values calculated from our simulated data in Pythia. These lines follow approximately the same path which gives confidence in the simulation by Pythia. We do not expect them to follow the exactly the same path as the theoretical values are calculated for the average between an interaction with a proton and an interaction with a neutron. Our simulations are for a proton only. The differences in the quark constituents for these two cases lead to the slightly differing paths. The raw data plotted in figure 6.31 is shown in table 6.2.

Energy	Simulated Value	Theoretical Value	Difference
100 GeV	0.5172	0.477	0.0402
1 TeV	0.4835	0.472	0.0115
10 TeV	0.4457	0.426	0.0197
100 TeV	0.3685	0.332	0.0365
1 PeV	0.2895	0.273	0.0165
10 PeV	0.2527	0.250	0.0027
100 PeV	0.2322	0.237	-0.0048
1 EeV	0.2195	0.225	-0.0055
10 EeV	0.1901	0.216	-0.0259
100 EeV	0.1433	0.208	-0.0647

Table 6.2: Our simulated values and theoretical values calculated by Gandhi *et al.* [10] for the y distribution.

6.4 Pion and kaon decay

Our results shown above concern the production of pions and kaons in a hadronic cascade resulting from an electron neutrino interaction. As these high energy pions and kaons travel through a medium they will lose energy and slow down by processes such as ionization before decaying.

The most probable decay modes and corresponding branching ratios for pions are shown in table 6.3. The charged pion decay to a muon has a high branching ratio of 99.99% and so we can assume that every charged pion will result in a muon.

The most probable decay modes and corresponding branching ratios for kaons are shown in table 6.4. These decay modes and branching ratios show that kaons do not

Decay mode	Branching ratio (%)
$\pi^\pm \rightarrow \mu^\pm + \nu_\mu$	99.99
$\pi^0 \rightarrow \gamma + \gamma$	98.80
$\pi^0 \rightarrow e^+ + e^- + \gamma$	1.20

Table 6.3: Decay modes with high branching ratios for pions [12].

always decay into muons. Although muons are their most common decay product the branching ratio for this decay mode is only 63.43%. However, it must also be noted that a kaon may have a decay product, such as a pion, which may then decay to a muon.

Decay mode	Branching ratio (%)
$K^\pm \rightarrow \mu^\pm + \nu_\mu$	63.43
$K^\pm \rightarrow \pi^0 + e^\pm + \nu_e$	4.87
$K^\pm \rightarrow \pi^0 + \mu^\pm + \nu_\mu$	3.27
$K^\pm \rightarrow \pi^\pm + \pi^0$	21.13
$K^\pm \rightarrow \pi^\pm + \pi^0 + \pi^0$	1.73
$K^\pm \rightarrow \pi^\pm + \pi^\pm + \pi^\mp$	5.58
$K_S^0 \rightarrow \pi^+ + \pi^-$	68.60
$K_S^0 \rightarrow \pi^0 + \pi^0$	31.40
$K_L^0 \rightarrow \pi^\pm + e^\mp + \nu_e$	38.79
$K_L^0 \rightarrow \pi^\pm + \mu^\mp + \nu_\mu$	27.18
$K_L^0 \rightarrow \pi^0 + \pi^0 + \pi^0$	21.08
$K_L^0 \rightarrow \pi^+ + \pi^- + \pi^0$	12.58

Table 6.4: Decay modes with high branching ratios for kaons [12].

Some pions will decay in flight to high energy muons but many will slow down to a stop. Negatively charged pions that are stationary may be captured by the Coulomb field of an atom in the surrounding medium. This occurs due to the central positive charge of the atom, and is called a pionic atom where the pion has taken the place of an electron [13]. This ‘particle’ is now analogous to a nucleon in an excited state, and loses energy by evaporation of low energetic particles or by leaving the nucleus. It is for this reason that we can expect far fewer negatively charged muons from charged pion decay than positively charged ones. The positive pions that decay from rest will decay into a positive muon with 109.82 MeV total energy. This is due to the rest mass of the pion being 139.57 MeV which must be shared between its decay products, the muon and the

muon neutrino. The muon neutrino takes 29.75 MeV of this energy, less than the muon since it is the lighter of these two decay products. We expect a peak in the number of muons produced from pion decay at 109.82 MeV since this is the only energy possible for the two bodied decay of a positive pion at rest.

6.5 Muon Production from Decay of Pions and Kaons

Our data produced from Pythia can be fed into GEANT using the inbuilt Pythia interface. Using this program the paths and processes of the particles produced in the hadronic cascade may then be simulated. Our simulated number of muons produced from the decay of pions and kaons for one electron neutrino event is shown in figures 6.32 to 6.39. These graphs show muon production for energies of 10 TeV, 100 TeV, 500 TeV and 1 PeV. Our simulated number of muons produced from the decay of pions and kaons for 100 electron neutrino events is shown in figures 6.40 to 6.43. These graphs show muon production for energies of 10 TeV and 100 TeV.

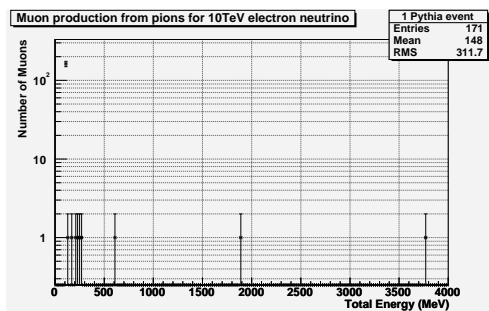


Figure 6.32: Muons from pion decay for one 10 TeV electron neutrino event.

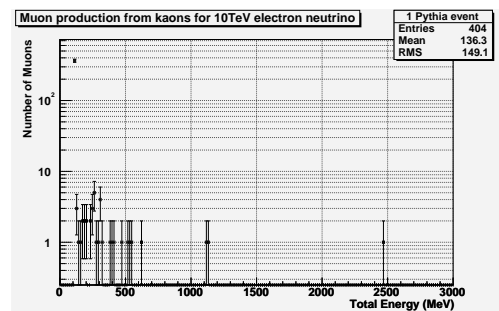


Figure 6.33: Muons from kaon decay for one 10 TeV electron neutrino event.

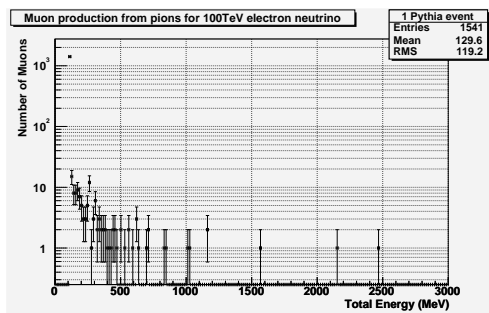


Figure 6.34: Muons from pions decay for one 100 TeV electron neutrino event.

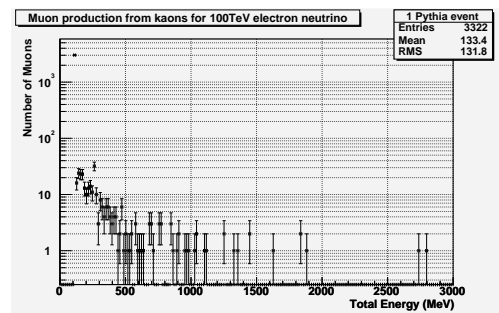


Figure 6.35: Muons from kaon decay for one 100 TeV electron neutrino event.

The data from our simulation of muon production from kaon decay for a 1 PeV incoming electron neutrino is somewhat smaller than other simulations. This is simply because each event is random and this one happens to have lower energy transferred to the hadronic cascade. Anomalies such as this are dealt with by running many events to improve the statistics. This is why we have run the higher event simulations.

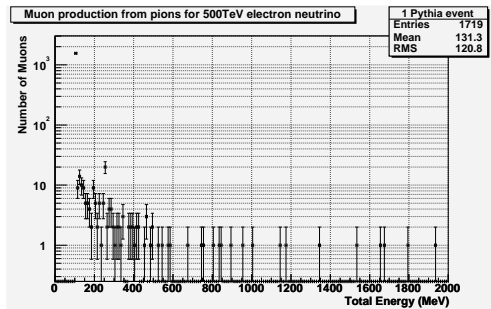


Figure 6.36: Muons from pion decay for one 500 TeV electron neutrino event.

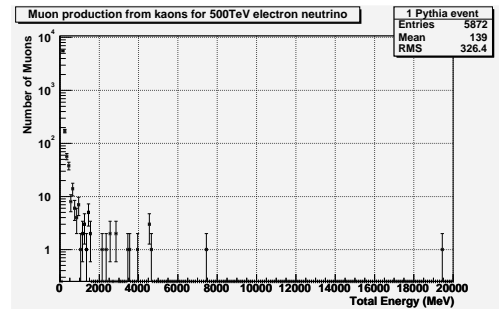


Figure 6.37: Muons from kaons decay for one 500 TeV electron neutrino event.

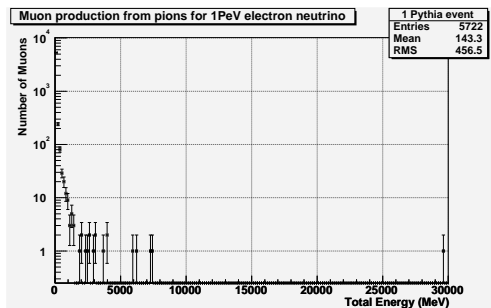


Figure 6.38: Muons from pion decay for one 1 PeV electron neutrino event.

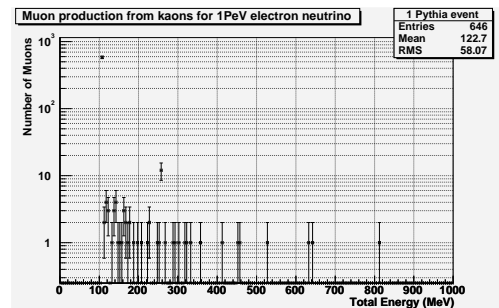


Figure 6.39: Muons from kaon decay for one 1 PeV electron neutrino event.

Attention must be drawn to the one hundred events simulation of muon production from kaon decay for an incoming electron neutrino energy of 10 TeV. This simulation contains the *highest* energy muon at 125.766 GeV. This simulation in particular demonstrates the possibility of extremely high energy long range muons resulting from an electron neutrino interaction. In this case the electron neutrino has only 10 TeV energy when it interacts in the ice. The muons path may be reconstructed and misinterpreted as a ‘fake’ muon event arising from a muon neutrino interaction, rather than an electron neutrino interaction.

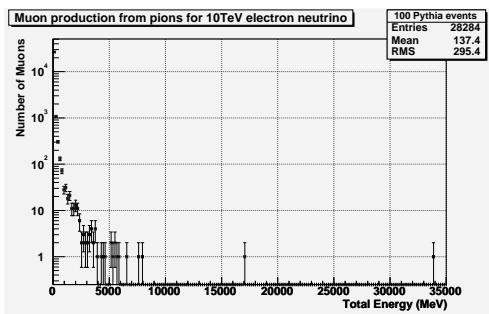


Figure 6.40: Muons from pion decay for one hundred 10 TeV electron neutrino events.

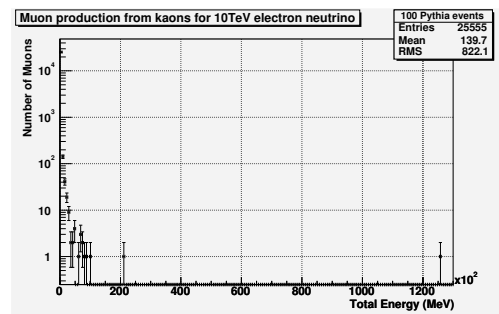


Figure 6.41: Muons from kaon decay for one hundred 10 TeV electron neutrino events.

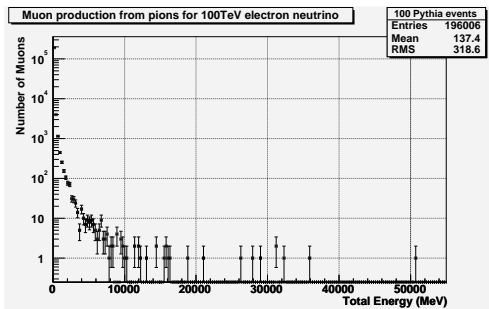


Figure 6.42: Muons from pion decay for one hundred 100 TeV electron neutrino events.

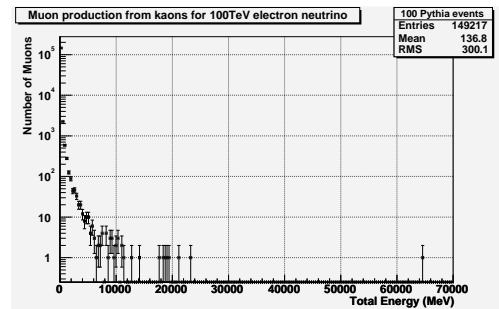


Figure 6.43: Muons from kaon decay for one hundred 100 TeV electron neutrino events.

Table 6.5 shows our simulated number of muons from pion and kaon decay and the mean energy of these muons. The mean energies simulated in GEANT are all approximately the same value of around 120 MeV to 150 MeV. This is low compared to the long range muons we are interested in due to the large number of low energy muons produced. It is the tail end of these graphs containing the very high energy muons that we are interested in.

	Energy	Number of muons		Mean energy of muon (MeV)	
		pion decay	kaon decay	pion decay	kaon decay
1 event	10 TeV	171	404	148.0	136.3
	100 TeV	1,541	3,322	129.6	133.4
	500 TeV	1,719	5,872	131.3	139.0
	1 PeV	5,722	646	143.3	122.7
100 events	10 TeV	28,284	25,555	137.4	134.8
	100 TeV	196,006	149,217	137.4	136.8

Table 6.5: Number of muons and their mean energies produced from pion and kaon decay.

Table 6.6 lists the three highest energy muons for each of our simulations. A significant number of long range muons have been produced even for low energy incoming electron neutrinos. The highest energy muon produced is given in italics.

	Energy	Highest energy muons (MeV)					
		from pion decay			from kaon decay		
1 event	10 TeV	3,764.1	1,894.5	601.6	2,464.6	1,132.9	1,114.5
	100 TeV	2,466.1	2,146.9	1,561.5	2,793.8	2,742.6	1,876.3
	500 TeV	1,933.8	1,792.6	1,677.8	19,476.7	7,401.4	4,671.0
	1 PeV	29,658.4	7,479.7	7,216.0	811.3	642.3	632.2
100 events	10 TeV	33,867.6	17,040.1	7,900.8	<i>125,766</i>	21,013.9	9,848.9
	100 TeV	36,018.3	32,232.6	31,338.8	64,535.1	23,278.5	21,235.1

Table 6.6: Highest energy muons from pion and kaon decay.

Chapter 7

Light Signal from Long Range Muons

Long range muons' signals in a neutrino detector are used in the reconstruction and analyse of neutrino events. In this chapter the timing of the light signal from long range muons is studied. This is to ascertain if the muon Cerenkov signal and the following event reconstruction is more complicated than originally thought.

7.1 Photons from long range muons

Muons travelling through a detector are long range particles [15]. Due to their mass of 105.7 MeV muons don't interact with the surrounding medium to emit a large number of Bremsstrahlung photons and lose energy as electrons do. Without this large energy loss muons travel a lot further before slowing down enough to cease emitting Cerenkov radiation. The signal detected by the digital optical modules (DOMs) must be understood in order to accurately reconstruct the muon's path through the detector.

The detection of the muons light is not as simple as one DOM after another receiving a photon. Each DOM may receive photons from two sources. The first is photons arising in the hadronic cascade produced in the initial neutrino interaction and the second is optical Cerenkov photons produced by the muon. All photons will travel at the local speed of light of the medium, $c_n = \frac{c}{n}$ where n is the refractive index, $n = 1.31$ for ice. However, the muon will travel close to the absolute speed of light in vacuum, a lot faster than the photons' speed. This will cause some DOMs to 'see' the muon before the hadronic cascade even though the hadronic cascade was the first event. With each DOM seeing the two events at a different time and in a different order, the reconstruction of the hadronic

cascade and the subsequent muon track can get very complicated.

The following calculations for the timing are a conservative estimate because the scattering of the photons has not been taken into account. It is a very good approximation to neglect scattering in the muon's path, however the scattering length for visible light in ice is approximately 5 m [8]. This scattering is for both the photons from the hadronic cascade and the photons from the Cerenkov light of the muon. The path from the hadronic cascade is always the longer one, so the resulting calculation is a conservative one. This will in practice, cause the area of light from the muon being received first to be more extensive than this calculation shows. These graphs show there is indeed an extensive region of DOMs in the detector that detect the light from the muon before the light from the hadronic cascade. This could make reconstruction of a electron neutrino event much more difficult than first anticipated.

7.2 Light signal simulation

We have run simulations to ascertain which DOMs receive the light from the muon first rather than the hadronic cascade. This simple program is written in C++ and it calculates the time difference between the two light signals at each of the DOMs point source locations. The DOMs are placed in a 1 km² array. This consists of nine strings, 125 m apart, each string has 60 DOMs spaced 17 m apart. The total array contains 540 DOM's. A muon neutrino interaction occurs at the coordinates (-125,500), half way down the array, and causes a hadronic cascade. A muon exits the cascade at varying angles and the timing of the two light signals for each DOM in the array is calculated. The source code is shown in appendix C.

This calculation is then displayed in two dimensional histograms. The results are shown in figures 7.1 to 7.10. These graphs range in the exiting angle for the muon from 10 degrees to 50 degrees. Our simulations were run for this angle clockwise and anticlockwise from the horizontal. In these graphs the calculated time difference is the difference between the light detected from the hadronic cascade minus the light detected from the muon to reach each DOM. This means the more negative this number, the earlier the light from the cascade reaches the DOM. This is represented by the bluer colouring on the graphs. The more positive this time difference the earlier the DOM 'sees' the light from the muon. This is represented by the redder colouring on the graphs.

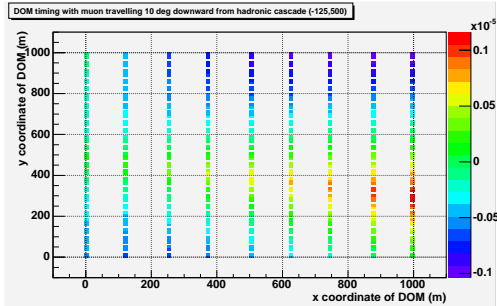


Figure 7.1: Muon travelling 10° downwards from (-125,500).

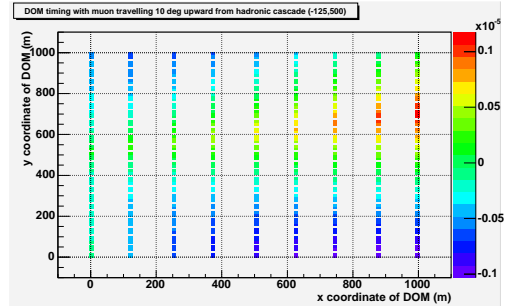


Figure 7.2: Muon travelling 10° upwards from (-125,500).

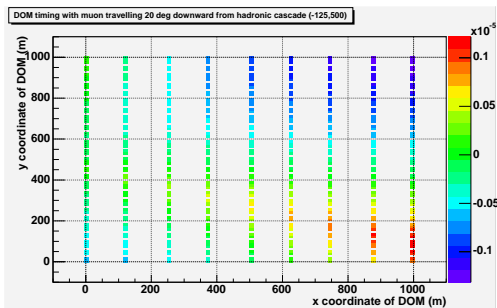


Figure 7.3: Muon travelling 20° downwards from (-125,500).

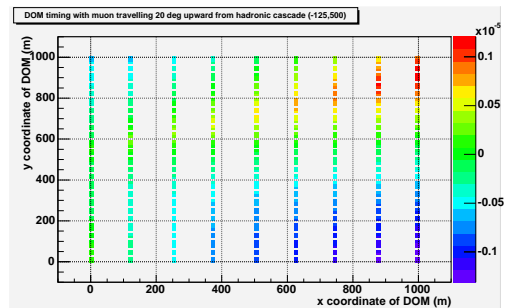


Figure 7.4: Muon travelling 20° upwards from (-125,500).

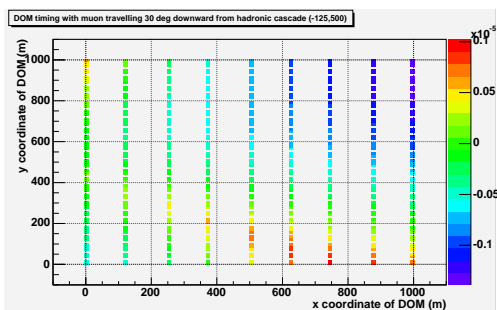


Figure 7.5: Muon travelling 30° downwards from (-125,500).

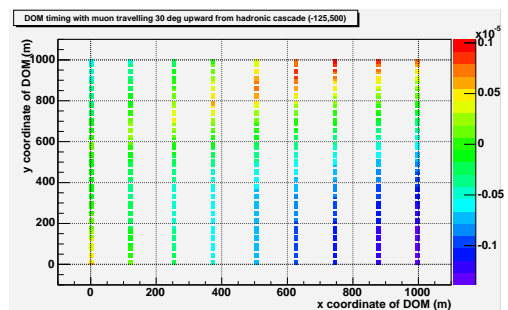


Figure 7.6: Muon travelling 30° upwards from (-125,500).

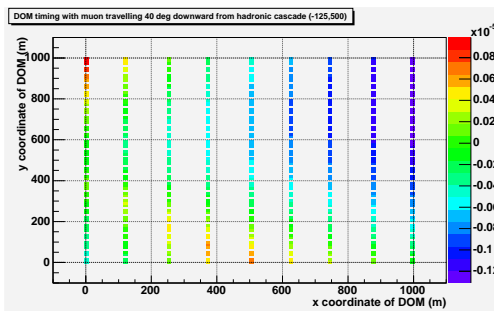


Figure 7.7: Muon travelling 40° downwards from $(-125,500)$.

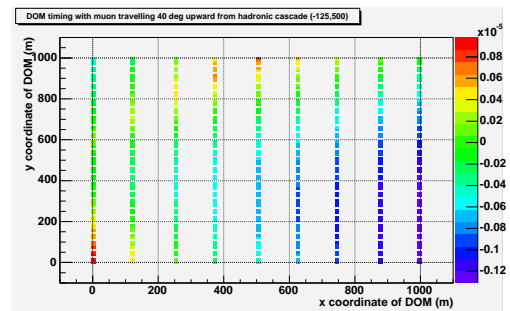


Figure 7.8: Muon travelling 40° upwards from $(-125,500)$.

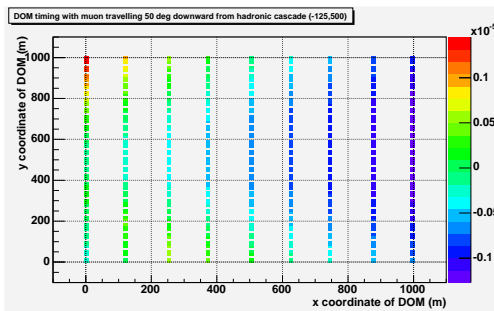


Figure 7.9: Muon travelling 50° downwards from $(-125,500)$.

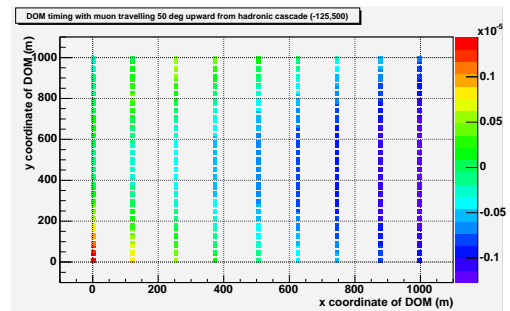


Figure 7.10: Muon travelling 50° upwards from $(-125,500)$.

Chapter 8

Summary and Conclusions

The use of neutrinos as a way to observe the universe has opened many windows in science. This weakly interacting particle allows us to look closer at gamma ray bursts, supernova bursts, active galactic nuclei, supernova remnants and to search for possible sources of high energy cosmic rays. We will learn more about neutrino oscillation and neutrinos as a possible WIMP candidate from the construction of large neutrino telescopes. Neutrino telescopes allows possible study of magnetic monopoles, other exotic particles including decay of super heavy particles and participation in the monitoring of supernova explosions for SNEWS. With the observation of high energy neutrinos it is hoped that new and unexpected phenomena will be discovered.

Neutrino interactions, which produce hadronic cascades and their charged lepton counterparts must be well understood. The three neutrino flavours each give distinct signals inside detectors. They each produce a unique Cerenkov distribution arising from the behaviour of their charged leptonic counterpart. Cerenkov radiation consists of a cone of light produced at a specific angle dependent on the phase refractive index of the medium, about 40 degrees in ice. The maximum number of Cerenkov optical photons produced per centimetre of track length was calculated to be to be 562 photons per cm.

The tau neutrino has not been exploited as an observation tool like the electron and muon neutrinos. This is because a larger detector effective area is required to raise the probability of a tau neutrino interaction in or near the detector. We have carried out simulations of this interaction for an event in ice as the medium. As expected from the tau lifetime, the tau produced in a tau neutrino interaction decayed very rapidly. We calculate that for tau to travel at least some observable distance across a detector it would have to enter with energy on the order of 1 PeV. We also carried out this simulation for muons in order to have a comparison between their Cerenkov distributions. Our simulations in-

cluded decay, multiple scattering, ionization, Bremsstrahlung, pair production and muon minus capture at rest for muons and decay, multiple scattering and ionization for tau. The Cerenkov distribution for tau shows double peaks due to the decay trajectory. The simulated number of Cerenkov optical photons per centimetre of track length for muons was found to be close to the theoretical calculation of 562 photons per cm.

As an electron neutrino enters a detector it interacts via or W^\pm boson exchange with a proton. This produces an electron, which initiates an electromagnetic cascade and a hadronic cascade resulting from the fragmentation of the constituents of the proton. The hadronic cascade may be very high energy, depending on how much energy from the original electron neutrino was taken. This may result in the hadrons in the cascade, including pions and kaons, having very high energy. In the situation that high energy pions and kaons decay into muons, the muons may be long range and appear to have originated from a muon neutrino interaction. This is called a ‘fake’ muon neutrino event. The probability of this occurring may be ascertained by running simulations. We have simulated the initial electron neutrino event and the particles produced in the subsequent hadronic cascade. We ran simulations for one event, one hundred events and ten thousand events. Many pions and kaons are produced in these hadronic cascades, some with very high energies. These simulations were verified by looking at the y distribution of the simulations and comparing it to theoretical values. This showed very good agreement with theoretical values calculated by Gandhi *et al.* [10].

We then propagated the pions and kaons produced in the hadronic cascade resulting from an electron neutrino event. GEANT 4.8 was used for this simulation with some additional physics added to the framework of the program. As expected we saw a peak in energy of the resulting muons at 109.82 MeV due to a phenomena called a pionic atom. However it is the other end of the distribution containing the high energy particles and therefore long range muons that we are interested in. Here we find many high energy muons. This confirms that indeed high energy pions and kaons produced in a hadronic cascade resulting from an electron neutrino interaction may decay to produce long range muons. These muons may be mistaken as arising from a muon neutrino event, hence are ‘fake’ muon neutrino events. The highest energy muon we observed in our simulations was over 125 GeV. This muon was produced when an electron neutrino of only 10 TeV interacted with a proton. It is important that neutrino telescopes pay attention to these high energy muons in their analyses. These long range muons in hadronic cascades can give us a handle on the direction of the incoming electron neutrino which may be otherwise difficult to ascertain.

We have shown that the reconstruction of electron neutrino cascades with long range muon may be more difficult than first anticipated. This is due to the muons velocity being faster than local speed of light in medium. The optical modules in a neutrino telescope detect the light signals from photons which travel much slower, at the local speed of light in the medium. This may cause difficulties to arise in the timing of events. We wrote a simple program to further study this problem. This program consists of a two dimensional array of digital optical modules arranged in a 1 km^2 block. A hadronic cascade occurs half way down the array and emits a long range muon. The time of travel of photons from the hadronic cascade and Cerenkov optical photons from the muon as it travels through the detector are calculated. The time difference between these two photons arrival at each digital optical module is then calculated. This has been plotted in two dimensional histograms with colour depicting the time difference. We indeed observe an extensive region of digital optical modules that ‘see’ the muon before the hadronic cascade even though the muon is the second event.

In this thesis we have studied some of the signals we expect to observe from each flavour of neutrino interaction with some interesting results which will affect the way we analyse neutrino telescope data. There is more work to be done in this area, which will allow us to take full advantage of the new observations offered by the neutrino window to the universe. There is still much more exciting science to carry out in this field. There will also be large amounts of data and analysis to carry out as we detect interaction of neutrinos from far outside our galaxy. This data and analysis will provide us with new science concerning existing phenomena and hopefully the discovery of new phenomena.

Appendix A

Additional physics source code

Listing A.1: Source code for the additional physics to the GEANT framework.

```
1 #include "G4ios.hh"
2 #include <iomanip>
3
4 #include "globals.hh"
5 #include "MyAdditionalPhysics.hh"
6
7 #include "G4ParticleDefinition.hh"
8 #include "G4ParticleTypes.hh"
9 #include "G4ParticleWithCuts.hh"
10 #include "G4ParticleTable.hh"
11
12 #include "G4Material.hh"
13 #include "G4MaterialTable.hh"
14
15 #include "G4ProcessManager.hh"
16 #include "G4ProcessVector.hh"
17
18 MyAdditionalPhysics::MyAdditionalPhysics(G4String aS) :
19     G4VPhysicsConstructor(aS) {}
20
21 MyAdditionalPhysics::~MyAdditionalPhysics() {}
22
23 void MyAdditionalPhysics::ConstructParticle()
24 {
25     G4OpticalPhoton::OpticalPhotonDefinition();
26 }
```

```

25
26 void MyAdditionalPhysics::ConstructProcess ()
27 {
28     ConstructOp ();
29 }
30
31 #include "G4Cerenkov.hh"
32 #include "G4OpAbsorption.hh"
33 #include "G4OpRayleigh.hh"
34 #include "G4OpBoundaryProcess.hh"
35
36 void MyAdditionalPhysics::ConstructOp ()
37 {
38     G4Cerenkov *theCerenkovProcess = new G4Cerenkov("Cerenkov");
39     //G4Scintillation *theScintillationProcess = new
40         G4Scintillation("Scintillation");
41     G4OpAbsorption *theAbsorptionProcess = new G4OpAbsorption();
42     G4OpRayleigh *theRayleighScatteringProcess = new G4OpRayleigh();
43     G4OpBoundaryProcess *theBoundaryProcess = new
44         G4OpBoundaryProcess();
45
46     //theCerenkovProcess->DumpPhysicsTable();
47     //theScintillationProcess->DumpPhysicsTable();
48     //theAbsorptionProcess->DumpPhysicsTable();
49     //theRayleighScatteringProcess->DumpPhysicsTable();
50
51     theCerenkovProcess->SetVerboseLevel(0);
52     //theScintillationProcess->SetVerboseLevel(0);
53     theAbsorptionProcess->SetVerboseLevel(0);
54     theRayleighScatteringProcess->SetVerboseLevel(0);
55     theBoundaryProcess->SetVerboseLevel(0);
56
57     //G4int MaxNumPhotons = 900;
58     //theCerenkovProcess->SetTrackSecondariesFirst(true);
59     //theCerenkovProcess->SetMaxNumPhotonsPerStep(MaxNumPhotons);
60
61     //theScintillationProcess->SetTrackSecondariesFirst(true);
62     //theScintillationProcess->SetScintillationYield(100./MeV);

```

```
61 //theScintillationProcess->SetResolutionScale(1.0);
62
63 G4OpticalSurfaceModel themodel = unified;
64 theBoundaryProcess->SetModel(themodel);
65
66 theParticleIterator->reset();
67 while((*theParticleIterator)()){
68 G4ParticleDefinition *particle = theParticleIterator->value();
69 G4ProcessManager *pmanager = particle->GetProcessManager();
70 G4String particleName = particle->GetParticleName();
71 if(theCerenkovProcess->IsApplicable(*particle)){
72 pmanager->AddContinuousProcess(theCerenkovProcess);
73 }
74 //if(theScintillationProcess->IsApplicable(*particle)){
75 //pmanager->AddProcess(theScintillationProcess);
76 //pmanager->SetProcessOrderingToLast(theScintillationProcess,
77 // idxAtRest);
78 //pmanager->SetProcessOrderingToLast(theScintillationProcess,
79 // idxPostStep);
80 //}
81 if(particleName == "opticalphoton"){
82 G4cout << "AddDiscreteProcess to OpticalPhoton" << G4endl;
83 pmanager->AddDiscreteProcess(theAbsorptionProcess);
84 pmanager->AddDiscreteProcess(theRayleighScatteringProcess);
85 pmanager->AddDiscreteProcess(theBoundaryProcess);
86 }
87 }
88 }
```

Appendix B

IceCube detector construction source code

Listing B.1: Source code for the IceCube detector construction.

```
1 #include "lightDetectorConstruction.hh"
2
3 #include "G4Material.hh"
4 #include "G4Box.hh"
5 #include "G4LogicalVolume.hh"
6 #include "G4ThreeVector.hh"
7 #include "G4PVPlacement.hh"
8
9 lightDetectorConstruction::lightDetectorConstruction()
10 : iceWorldLogical(0), iceWorldPhysical(0)
11 {}
12
13 lightDetectorConstruction::~~lightDetectorConstruction()
14 {}
15
16 G4VPhysicalVolume* lightDetectorConstruction::Construct()
17 {
18
19 //-----MATERIALS-----
20
21     G4double a;                               //atomic mass
22
23     a = 1.01*g/mole;
```

```

24  G4Element* elH = new G4Element("Hydrogen", "H", 1, a);
25
26  a = 16.00*g/mole;
27  G4Element* elO = new G4Element("Oxygen", "O", 8, a);
28
29  G4Material* H2O = new G4Material("Ice", 0.9168*g/cm3, 2, kStateSolid);
30  H2O->AddElement(elH, 2);
31  H2O->AddElement(elO, 1);
32
33  //-----VOLUMES-----
34
35  //-----Block Of Ice (World Volume)-----
36  //-----Beam Line Along x Axis-----
37
38  G4Box* iceWorldBox = new G4Box("Ice_world_
    box", 10000*m, 10000*m, 10000*m);
39  iceWorldLogical = new G4LogicalVolume(iceWorldBox, H2O, "Ice_world_
    logical", 0, 0, 0);
40  iceWorldPhysical = new G4PVPlacement(0, G4ThreeVector(), "Ice_
    world", iceWorldLogical, 0, false, 0);
41
42  //////////////////////////////////////
43  //          Generate & Add Material Properties Table          //
44  //////////////////////////////////////
45
46  const G4int NUMENTRIES = 32;
47
48  G4double PPCKOV[NUMENTRIES] =
49  { 2.034E-9*GeV, 2.068E-9*GeV, 2.103E-9*GeV, 2.139E-9*GeV,
50    2.177E-9*GeV, 2.216E-9*GeV, 2.256E-9*GeV, 2.298E-9*GeV,
51    2.341E-9*GeV, 2.386E-9*GeV, 2.433E-9*GeV, 2.481E-9*GeV,
52    2.532E-9*GeV, 2.585E-9*GeV, 2.640E-9*GeV, 2.697E-9*GeV,
53    2.757E-9*GeV, 2.820E-9*GeV, 2.885E-9*GeV, 2.954E-9*GeV,
54    3.026E-9*GeV, 3.102E-9*GeV, 3.181E-9*GeV, 3.265E-9*GeV,
55    3.353E-9*GeV, 3.446E-9*GeV, 3.545E-9*GeV, 3.649E-9*GeV,
56    3.760E-9*GeV, 3.877E-9*GeV, 4.002E-9*GeV, 4.136E-9*GeV };
57
58  G4double RINDEX1[NUMENTRIES] =

```

```

59     { 1.31, 1.31, 1.31, 1.31, 1.31, 1.31, 1.31, 1.31, 1.31, 1.31,
60         1.31, 1.31, 1.31, 1.31, 1.31, 1.31, 1.32, 1.32, 1.32, 1.32,
61         1.32, 1.32, 1.32, 1.32, 1.32, 1.32, 1.32, 1.33, 1.33, 1.33,
62         1.33, 1.33 };
63
64 G4double ABSORPTION1[NUMENTRIES] =
65     { 344.8*cm, 408.2*cm, 632.9*cm, 917.4*cm, 1234.6*cm,
66         1388.9*cm, 1515.2*cm, 1724.1*cm, 1886.8*cm, 2000.0*cm,
67         2631.6*cm, 3571.4*cm, 4545.5*cm, 4761.9*cm, 5263.2*cm,
68         5263.2*cm, 5555.6*cm, 5263.2*cm, 5263.2*cm, 4761.9*cm,
69         4545.5*cm, 4166.7*cm, 3703.7*cm, 3333.3*cm, 3000.0*cm,
70         2850.0*cm, 2700.0*cm, 2450.0*cm, 2200.0*cm, 1950.0*cm,
71         1750.0*cm, 1450.0*cm };
72
73 G4MaterialPropertiesTable *myMPT1 = new
74     G4MaterialPropertiesTable();
75 myMPT1->AddProperty("RINDEX",PPCKOV,RINDEX1,NUMENTRIES);
76 myMPT1->AddProperty("ABSLENGTH",PPCKOV,ABSORPTION1,NUMENTRIES);
77 H2O->SetMaterialPropertiesTable(myMPT1);
78
79 const G4int NUM = 2;
80 G4double PP[NUM] =
81     { 1.001E-9*GeV, 4.144E-9*GeV };
82 G4double RINDEX[NUM] =
83     { 1.30, 1.34 };
84 G4double SPECULARLOBECONSTANT[NUM] =
85     { 0.3, 0.3 };
86 G4double SPECULARSPIKECONSTANT[NUM] =
87     { 0.2, 0.2 };
88 G4double BACKSCATTERCONSTANT[NUM] =
89     { 0.2, 0.2 };
90
91 G4MaterialPropertiesTable *myST1 = new G4MaterialPropertiesTable();
92 myST1->AddProperty("RINDEX",PP,RINDEX,NUM);
93 myST1->AddProperty("SPECULARLOBECONSTANT",PP,SPECULARLOBECONSTANT,
94     NUM);
95 myST1->AddProperty("SPECULARSPIKECONSTANT",PP,SPECULARSPIKECONSTANT,
96     NUM);

```

```
94 myST1->AddProperty("BACKSCATTERCONSTANT",PP,BACKSCATTERCONSTANT,
    NUM);
95
96 G4double REFLECTIVITY[NUM] =
97     { 0.3, 0.5 };
98 G4double EFFICIENCY[NUM] =
99     { 0.8, 1.0 };
100
101 G4MaterialPropertiesTable *myST2 = new G4MaterialPropertiesTable();
102 myST2->AddProperty("REFLECTIVITY",PP,REFLECTIVITY,NUM);
103 myST2->AddProperty("EFFICIENCY",PP,EFFICIENCY,NUM);
104
105 return iceWorldPhysical;
106 }
```

Appendix C

DOM timing source code

Listing C.1: Source code for DOM timing of long range muon tracks.

```
1 //CALCULATING THE TIMING OF LIGHT FROM CASCADE AND MUON REACHING EACH
   DOM
2
3 #include <stdio.h>
4 #include <stdlib.h>
5 #include <math.h>
6 #define PI 3.14159265
7
8 int main(void)
9 {
10
11 //DEFINITIONS
12
13 double c; //absolute speed of light
14 double c_n; //speed of light in medium (c/n where n=1.31)
15 double theta; //angle muon travels from zero
16 int NoDOM; //Number of DOM
17 int DOMX[16]; //digital optical modul x coordinate
18 int DOMY[16]; //digital optical module y coordinate
19 double dummy;
20 double x;
21 int HCX; //hadronic cascade x coordinate
22 int HCY; //hadronic cascade y coordinate
23 double phi; //angle DOM is from zero
24 double angle; //angle of triangle (theta - phi)
```

```

25  double d_c;      //distance from hadronic cascade to DOM
26  double d_m;      //distance muon travels until perbendicular to DOM
27  double d_l;      //distance light from muon travels to DOM
28  double t_c;      //time for light from hadronic cascade to reach DOM
29  double t_m;      //time for muon travel until perbendicular to DOM
30  double t_l;      //time for light from muon to reach DOM
31  double t_lm;     //total time for light from muon to reach DOM (t_m
      + t_l)
32  double dt;      //time difference between two paths (t_c - t_lm)
33
34  //MAIN
35
36  //set absolute speed of light (ms-1)
37  c = 2.99792458E+08;
38  //set speed of light in medium (ms-1)
39  c_n = 2.288492046E+08;
40  //give a value for angle that muon travels from zero (deg)
41  theta = 10*(PI/180);
42  //label each DOM with position (m)
43  for (NoDOM=0; NoDOM<16; ++NoDOM) {
44      DOMX[NoDOM] = (NoDOM%4)*125;
45      dummy = modf(NoDOM/4,&x);
46      DOMY[NoDOM] = x*17;
47  }
48  //give hadronic cascade position (m)
49  HCX = -125;
50  HCY = 34;
51
52  //Set loop for each DOM
53  for (NoDOM=0; NoDOM<16; ++NoDOM) {
54      //calculate angle DOM is from zero (deg)
55      phi = atan((double) (HCY-DOMY[NoDOM]) / (double) (DOMX[NoDOM]-HCX));
56      //calculate angle of triangle (deg)
57      angle = fabs(phi-theta);
58      //calculate distance from hadronic cascade to DOM (m)
59      d_c = sqrt((double)pow(HCY-DOMY[NoDOM],2) +
      (double)pow(DOMX[NoDOM]-HCX,2));
60      //calculate distance muon travels until perbendicular to DOM (m)

```

```
61     d_m = d_c*cos(angle);
62     //calculate distance light from muon travels to DOM (m)
63     d_l = d_c*sin(angle);
64     //calculate time for light from hadronic cascade to reach DOM (s)
65     t_c = d_c/c_n;
66     //calculate time for muon travel until perpendicular to DOM (s)
67     t_m = d_m/c;
68     //calculate time for light from muon to reach DOM (s)
69     t_l = d_l/c_n;
70     //calculate total time for light from muon to reach DOM (s)
71     t_lm = t_m+t_l;
72     //calculate time difference between two paths (s)
73     dt = t_c-t_lm;
74
75     printf("%4d",DOMX[NoDOM]);
76     printf("%4d",DOMY[NoDOM]);
77     printf("%14e",dt);
78     printf("\n");
79 }
80 return 0;
81 }
```

Bibliography

- [1] IceCube Neutrino Observatory. <http://icecube.wisc.edu/>, February 2007.
- [2] Nestor - Scientific Programme. http://www.nestor.org.gr/programme/nestor__scientific_programme.htm, February 2007.
- [3] Barwick Group. Amanda II Project - Official Site. <http://amanda.uci.edu/>, 9th September 2005.
- [4] R. Bionta, G. Blewitt, C. Bratton, D. Casper, A. Ciocio, R. Claus, B. Cortez, M. Crouch, S. Dye, S. Errede, et al. Observation of a neutrino burst in coincidence with supernova 1987A in the Large Magellanic Cloud. *Physical Review Letters*, 58(14):1494–1496, 1987.
- [5] R. Brun, R. Hagelberg, M. Hansroul, and J. Lassalle. GEANT: Simulation Program for Particle Physics Experiments. User Guide and Reference Manual. *CERN Rep. CERN-DD-78-2*, July, 1978.
- [6] P. Cerenkov. Visible radiation produced by electrons moving in a medium with velocities exceeding that of light. *Phys. Rev.*, 52:378–379, 1937.
- [7] D. Etter. *Structured FORTRAN 77 for engineers and scientists*. Benjamin/Cummings Redwood City, Calif, 1990.
- [8] I. Fermin. *Search for High Energy Neutrino Induced Cascades with the AMANDA-B10 Detector*. PhD thesis, University of Pennsylvania, 2002.
- [9] T. Gaisser. *Cosmic Rays and Particle Physics*. Cambridge University Press, 1990.
- [10] R. Gandhi, C. Quigg, M. Reno, and I. Sarcevic. Ultrahigh-Energy Neutrino Interactions. *Arxiv preprint hep-ph/9512364*, 1995.

- [11] S. Giani et al. Geant4: An object-oriented toolkit for simulation in HEP. *CERN/L-HCC*, pages 98–44, 1998.
- [12] K. Hagiwara et al. *Review of Particle Physics*, volume 66. 2002.
- [13] K. Han. Simulation of Cascades Using GEANT4 for IceCube. 2005.
- [14] K. Hirata, T. Kajita, M. Koshiba, M. Nakahata, Y. Oyama, N. Sato, A. Suzuki, M. Takita, Y. Totsuka, T. Kifune, et al. Observation of a neutrino burst from the supernova SN1987A. *Physical Review Letters*, 58(14):1490–1493, 1987.
- [15] IceCube Collaboration. *IceCube Preliminary Design Document*, 1.24 edition, October 2001.
- [16] J. Jackson and R. Fox. *Classical Electrodynamics*, volume 67. AAPT, 1999.
- [17] J. G. Learned. The DUMAND Project. <http://www.phys.hawaii.edu/~dumand/>, 2nd June 2003.
- [18] P. Miocinovic. *Muon energy reconstruction in the Antarctic Muon And Neutrino Detector Array (AMANDA)*. PhD thesis, UNIVERSITY of CALIFORNIA, 2001.
- [19] D. Perkins. *Introduction to High Energy Physics*. Cambridge University Press, 2000.
- [20] P. B. Price and K. Woschnagg. Role of group and phase velocity in high-energy neutrino observatories. *Astropart. Phys.*, 15:97–100, 2001.
- [21] F. Reines and C. Cowan. The Neutrino. *Nature*, 178(4531):446–449, 1956.
- [22] T. Sjöstrand, L. Lönnblad, and S. Mrenna. *PYTHIA 6.2 Physics and Manual*, 2001.
- [23] G. Smith. *An Introduction to Classical Electromagnetic Radiation*. Cambridge University Press, 1997.
- [24] T. Stolarczyk. ANTARES home page. <http://antares.in2p3.fr/>, February 2007.
- [25] O. Streicher. Baikal Home Page. <http://www.ifh.de/baikal/baikalhome.html>, 16th May 1995.
- [26] C. Wiebusch. *The Detection of Faint Light in Deep Underwater Neutrino Telescopes*. PhD thesis, Physikalische Inst, 1995.

Acknowledgements

This thesis would not have been possible without my supervisors: Assoc. Prof. Mike Reid, Dr. Jennifer Adams and Dr. Surujhdeo Seunarine. They introduced me to neutrino particle physics and the IceCube project, and have been a constant source of help and inspiration. Their support and enthusiasm has been much appreciated throughout my Masters studies.

Thanks to mum and dad for their time and effort proof reading and their ongoing encouragement. I would also like to thank my office mates, especially Richard Graham for all his patience and support with computing.